

**AD-A252 851**



2

PL-TR-92-2034

## **Formation and Propagation of Love Waves from a P-wave Source**

S. A. Miller  
A. L. Florence  
S. W. Kirkpatrick

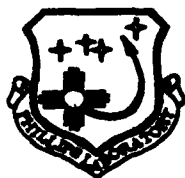
SRI International  
333 Ravenswood Avenue  
Menlo Park, CA 94025-3493

January 1992

Final Report  
January 25, 1989 - January 31, 1992

DTIC  
SELECTE  
MAY 27 1992  
S B D

Approved for public release; distribution unlimited



PHILLIPS LABORATORY  
AIR FORCE SYSTEMS COMMAND  
HANSCOM AFB, MASSACHUSETTS 01731-5000

**92-13848**




92 5 26 063


SPONSORED BY  
Defense Advanced Research Projects Agency  
Nuclear Monitoring Research Office  
ARPA ORDER NO. 5307

MONITORED BY  
Phillips Laboratory  
Contract F19628-89-K-0009

The views and conclusions contained in this document are those of the authors and should not be interpreted as representing the official policies, either expressed or implied, of the Defense Advanced Research Projects Agency or the U.S. Government.

This technical report has been reviewed and is approved for publication.

  
JAMES F. LEWKOWICZ  
Contract Manager  
Solid Earth Geophysics Branch  
Earth Sciences Division

  
JAMES F. LEWKOWICZ  
Branch Chief  
Solid Earth Geophysics Branch  
Earth Sciences Division

  
DONALD H. ECKHARDT, Director  
Earth Sciences Division

This report has been reviewed by the ESD Public Affairs Office (PA) and is releasable to the National Technical Information Service (NTIS).

Qualified requestors may obtain additional copies from the Defense Technical Information Center. All others should apply to the National Technical Information Service.

If your address has changed, or if you wish to be removed from the mailing list, or if the addressee is no longer employed by your organization, please notify PL/IMA, Hanscom AFB, MA 01731-5000. This will assist us in maintaining a current mailing list.

Do not return copies of this report unless contractual obligations or notices on a specific document requires that it be returned.

REPORT DOCUMENTATION PAGE			Form Approved OMB No. 0704-0188	
<small>Public reporting burden for this collection of information is estimated to average 1 hour per response, including the time for reviewing instructions, searching existing data sources, gathering and maintaining the data needed, and completing and reviewing the collection of information. Send comments regarding this burden estimate or any other aspect of this collection of information, including suggestions for reducing the burden, to Washington Headquarters Service, Directorate for Information Operations and Reports, 1215 Jefferson Davis Highway, Suite 1204, Arlington, VA 22202-4302, and to the Office of Management and Budget, Paperwork Reduction Project (0704-0188), Washington, DC 20503</small>				
1. AGENCY USE ONLY (Leave blank)		2. REPORT DATE January 1992	3. REPORT TYPE AND DATES COVERED Final Report - 890125-920131	
4. TITLE AND SUBTITLE Formation and Propagation of Love Waves from a P-Wave Source			5. FUNDING NUMBERS PE 62714E PR 9A10 TA DA WU BB  Contract F19628-89-K-0009	
6. AUTHOR(S) A. L. Florence S. A. Miller S. W. Kirkpatrick				
7. PERFORMING ORGANIZATION NAME(S) AND ADDRESS(ES) SRI International 333 Ravenswood Avenue Menlo Park, CA 94025			8. PERFORMING ORGANIZATION REPORT NUMBER  SRI Project 7206	
9. SPONSORING/MONITORING AGENCY NAME(S) AND ADDRESS(ES) Phillips Laboratory Hanscom AFB Massachusetts 01731-5000  Contract Manager: James Lewkowicz/GPEH			10. SPONSORING/MONITORING AGENCY REPORT NUMBER  PL-TR-92-2034	
11. SUPPLEMENTARY NOTES				
12a. DISTRIBUTION/AVAILABILITY STATEMENT  Approved for public release; distribution unlimited.			12b. DISTRIBUTION CODE	
13. ABSTRACT (Maximum 200 words) The objective of this research is to investigate experimentally, and support by finite element calculations, the formation and propagation of Love waves from a P-wave source due to scattering at material heterogeneities. We conducted a series of experiments where surface strains were measured parallel and perpendicular to a planar granite scattering surface. The granite wall cast in a surface layer waveguide of a low-impedance grout and then cast on a granite base provided the interface for generating horizontally polarized (SH) waves in the surface layer. The in-plane shear waves are the Love waves we measured at the surface. The P-wave source was a 1-cm-diameter spherical explosive of PETN diluted with microballoons to provide a charge density of 0.45 g/cm cast in a styrofoam sphere to further attenuate the peak pressure. We successfully measured the strains at three locations parallel to the wall and two locations perpendicular to the wall, and the test repeatability was good. Good agreement was also observed between the measured and calculated strain at all locations. The code calculations also showed that in-plane shear strains form along the surface layer/granite interface, and these shear strains propagate				
14. SUBJECT TERMS P-waves Love waves Heterogeneities			15. NUMBER OF PAGES 54	
			16. PRICE CODE	
17. SECURITY CLASSIFICATION OF REPORT  Unclassified	18. SECURITY CLASSIFICATION OF THIS PAGE  Unclassified	19. SECURITY CLASSIFICATION OF ABSTRACT  Unclassified	20. LIMITATION OF ABSTRACT  SAR	

UNCLASSIFIED

SECURITY CLASSIFICATION OF THIS PAGE

CLASSIFIED BY:

DECLASSIFY ON:

CONT. of Block 13:

with little reduction in amplitude but transform relatively high-frequency oscillations to low-frequency wave packets.

In this report, we present the experimental configuration used to generate and measure Love waves, an evaluation of the source used in the surface layer experiments, and results from finite element code calculations of the experiment.

SECURITY CLASSIFICATION OF THIS PAGE

## CONTENTS

Section	Page
ILLUSTRATIONS .....	iv
SUMMARY .....	vii
PREFACE .....	ix
1 OBJECTIVE AND APPROACH .....	1
1.1 Evaluation of the Source .....	1
1.2 Source Evaluation Experiment .....	4
2 SURFACE WAVE EXPERIMENT AND CALCULATION .....	10
2.1 Finite Element Calculations .....	10
2.2 Comparison of Experiments and Calculation .....	17
3 CONCLUSIONS .....	28
4 REFERENCES .....	29
APPENDIX A .....	31



<b>Accession For</b>	
NTIS GRA&I	<input checked="" type="checkbox"/>
DTIC TAB	<input type="checkbox"/>
Unannounced	<input type="checkbox"/>
Justification	
By _____	
Distribution/	
Availability Codes	
Dist  A-1	Avail and/or Special

## ILLUSTRATIONS

Figure		Page
1	Configuration for surface wave experiments .....	2
2	Source configuration used in surface wave experiments .....	3
3	Configuration of source evaluation experiment .....	5
4	Particle velocity histories measured in source evaluation experiment .....	7
5	Displacement histories measured in source evaluation experiment .....	8
6	Radial and circumferential surface strain histories measured in source evaluation experiment .....	9
7	Gage layout and configuration of surface wave experiments .....	11
8	Velocity boundary condition at 2-cm range input to finite element calculations .....	12
9	Finite element meshes .....	14
10	Top view of fringes of x-y surface shear strain for calculation without the wall (layer over half-space) .....	15
11	Top view of fringes of x-y surface shear strain in calculation with the wall .....	16
12	Fringes of pressure at 75 $\mu$ s for calculation with the wall .....	18
13	Effect of wall on strain in direction perpendicular to wall .....	19
14	Measured and calculated surface strain histories at Station A (5.1-cm range parallel to wall) in surface wave experiments .....	20
15	Measured and calculated surface strain histories at Station B (10.2-cm range parallel to wall) in surface wave experiments .....	21
16	Measured and calculated surface strain histories at Station C (20.3-cm range parallel to wall) in surface wave experiments .....	22
17	Measured and calculated surface strain histories at Station D (5.1-cm range perpendicular to wall) in surface wave experiments .....	23

## ILLUSTRATIONS (CONTINUED)

Figure		Page
18	Measured and calculated surface strain histories at Station F (20.3-cm range perpendicular to wall) in surface wave experiments .....	24
19	Comparison of calculated x-y shear strain parallel and perpendicular to wall .....	26
20	Calculated Love waves at Stations A, B, and C .....	27
A.1	Measured surface strain histories at Station A (5.1-cm range parallel to wall) in surface wave experiments .....	A-2
A.2	Measured surface strain histories at Station B (10.2-cm range parallel to wall) in surface wave experiments .....	A-3
A.3	Measured surface strain histories at Station C (20.3-cm range parallel to wall) in surface wave experiments .....	A-4
A.4	Measured surface strain histories at Station D (5.1-cm range perpendicular to wall) in surface wave experiments .....	A-5
A.5	Measured surface strain histories at Station F (20.3-cm range perpendicular to wall) in surface wave experiments .....	A-6

## SUMMARY

The objective of this research is to investigate experimentally, and support by finite element calculations, the formation and propagation of Love waves from a P-wave source due to scattering at material heterogeneities. We conducted a series of experiments where surface strains were measured parallel and perpendicular to a planar granite scattering surface. The granite wall cast in a surface layer waveguide of a low-impedance grout and then cast on a granite base provided the interface for generating horizontally polarized (SH) waves in the surface layer. The in-plane shear waves are the Love waves we measured at the surface. The P-wave source was a 1-cm-diameter spherical explosive of PETN diluted with microballoons to provide a charge density of  $0.45 \text{ g/cm}^3$  cast in a styrofoam sphere to further attenuate the peak pressure. We successfully measured the strains at three locations parallel to the wall and two locations perpendicular to the wall, and the test repeatability was good. Good agreement was also observed between the measured and calculated strain at all locations. The code calculations also showed that in-plane shear strains form along the surface layer/granite interface, and these shear strains propagate with little reduction in amplitude but transform relatively high-frequency oscillations to low-frequency wave packets.

In this report, we present the experimental configuration used to generate and measure Love waves, an evaluation of the source used in the surface layer experiments, and results from finite element code calculations of the experiment.



## **PREFACE**

This research was conducted under Contract F19628-89-K-0009 sponsored by DARPA (DoD) and issued by the Earth Sciences Division, Geophysics Directorate, of the Phillips Laboratory. The technical monitor was Mr. James F. Lewkowicz.

The authors are indebted to the following personnel at SRI International who contributed to the program: E. M. Oyola for preparation and performance of the experiments, M. A. Merritt for instrumentation, and F. B. Galimba for sensor installation.

## SECTION 1

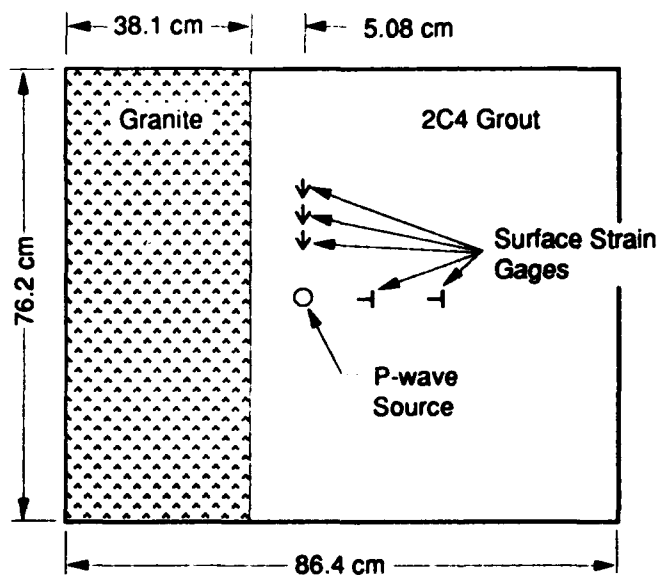
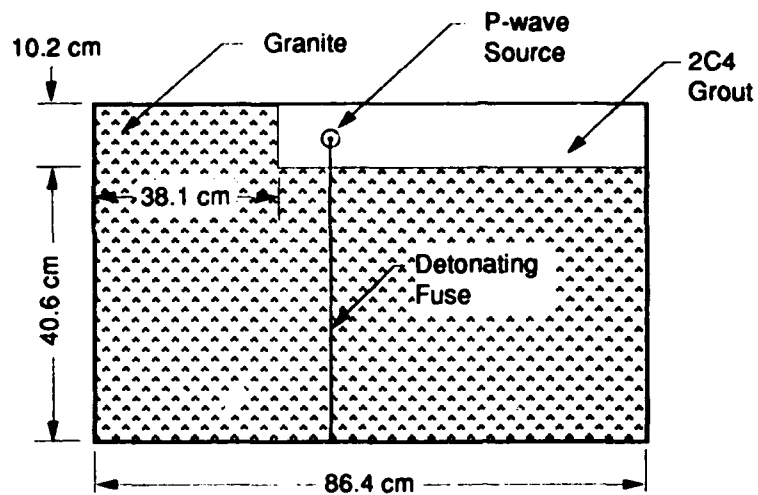
### OBJECTIVE AND APPROACH

Detection of underground nuclear explosions includes the spectral analysis of seismograms, an important portion of which is the contribution of Love waves. Field evidence suggests that it may be possible to discriminate between nuclear events and earthquakes by examining the Love wave records. The spectra for these events are different because an earthquake generates shear waves directly, whereas an underground explosion generates P-waves, from which Love waves are produced by scattering from material heterogeneities. Our objective in this research was to produce experimental evidence of the formation and propagation of Love waves in small-scale laboratory experiments, and analyze the resulting records with finite element calculations of each experiment. The approach is shown schematically in Figure 1. In these experiments, a heterogeneous scattering surface in the form of a vertical planar wall is cast into the surface layer, converting incident P-wave energy into shear waves. Shear waves are reflected at the interface between the granite and the lower-impedance 2C4 grout interface, and the horizontally polarized shear waves (SH-wave) generated at the wall and trapped in the surface layer waveguide are the Love waves. In the experiments, we measured the propagated surface strains of the undisturbed signal and signals modified by scattering. We compared the measured and calculated strains to establish agreement and used to calculations to examine the Love waves produced by the vertical planar interface.

#### 1.1 EVALUATION OF THE SOURCE

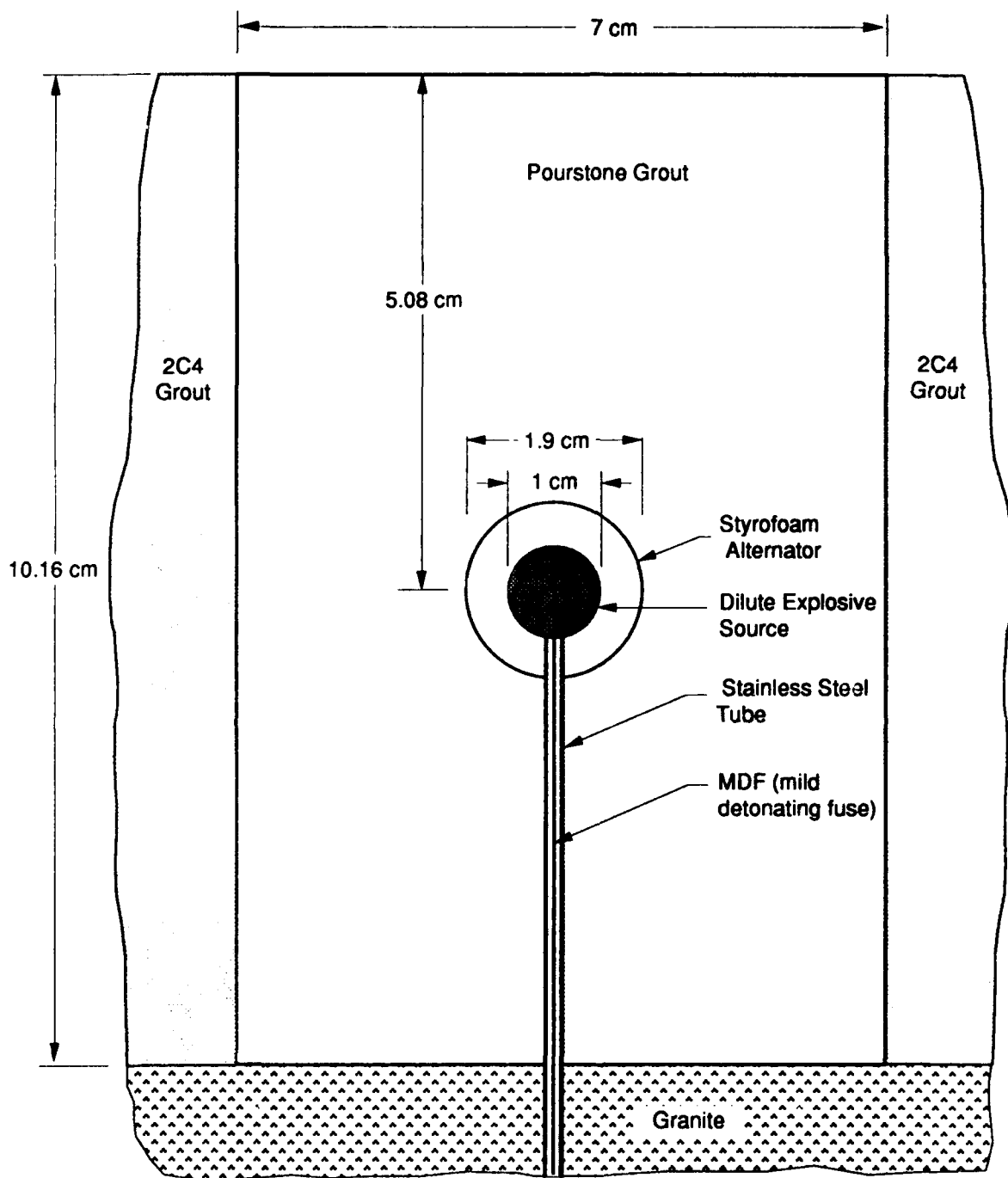
Initially, we investigated a spherical piezoelectric crystal as the P-wave source. The results of our investigation, expanded in a separate report<sup>1</sup> showed this source to be inadequate for generating signals of high enough amplitude at the longer ranges of interest, especially after scattering, to be easily resolved by measurements at the surface. The piezoelectric crystal approach may still prove useful; however, a significant effort in development of higher-output power supplies is required.

An alternative to the piezoelectric source was developed and is shown schematically in Figure 2. This source is a modification to the spherical explosive charge used in previous efforts.<sup>2</sup> The source consists of a PETN explosive diluted by spherical plastic beads (called microballoons) encased in an acrylic sphere. The density of the dilute explosive is  $0.45 \text{ g/cm}^3$ , formulated by combining 97% by weight PETN and 3% by



RM-7206-28

Figure 1. Configuration for surface wave experiments.



RM-7206-29

Figure 2. Source configuration used in surface wave experiments.

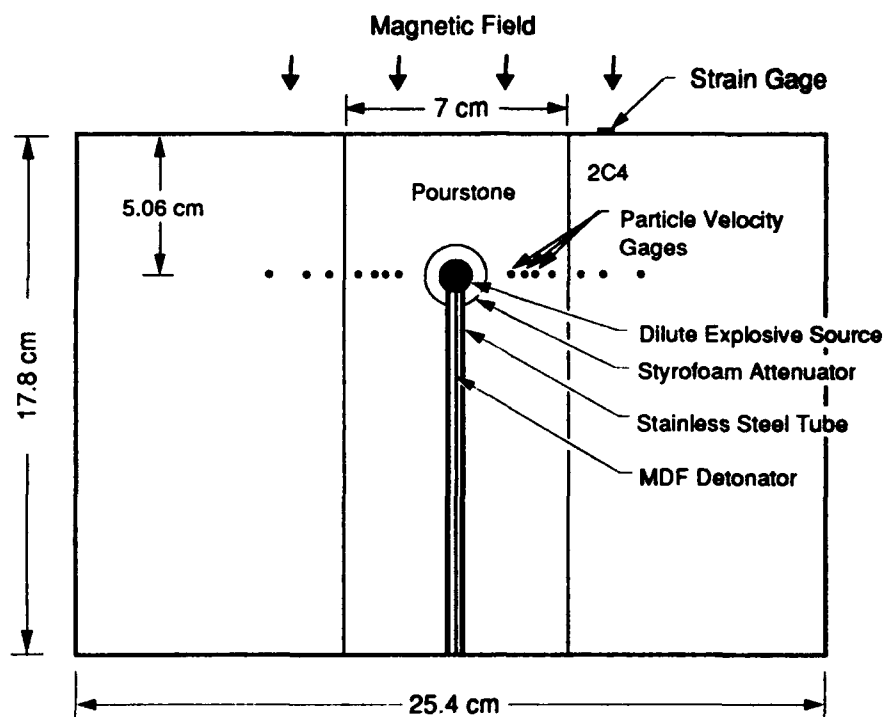
weight microballoons. The lower charge density reduces the Chapman-Jouguet (C-J) pressure of the source from about 7.5 GPa for our typical 1.0 g/cm<sup>3</sup> PETN density to about 1.0 GPa for the dilute charge.<sup>3</sup> We performed an experiment like that shown in Figure 1 using a dilute explosive source coupled directly to the pourstone grout. Unfortunately, this source was too energetic and caused significant surface spall in the model. Consequently, we made a final modification to the source by encasing the dilute charge in a 1.19-cm styrofoam sphere to further attenuate the peak pressure before propagating into the surface layer material. The source was detonated by 2 grain/ft mild detonating fuse running from the bottom of the specimen confined by a stainless steel tube.

Another consideration in the design of the source was efficient source installation between experiments. The surface layer material is 2C4 grout; however, because this grout has a substantial curing time, 90% strength at 28 days, we instead used pourstone to cast the source into the surface layer model because it cures in about 2 hours. Between experiments, we cored out the old source and cast in the new source with pourstone. The properties of pourstone match closely with the properties of the 2C4 grout.

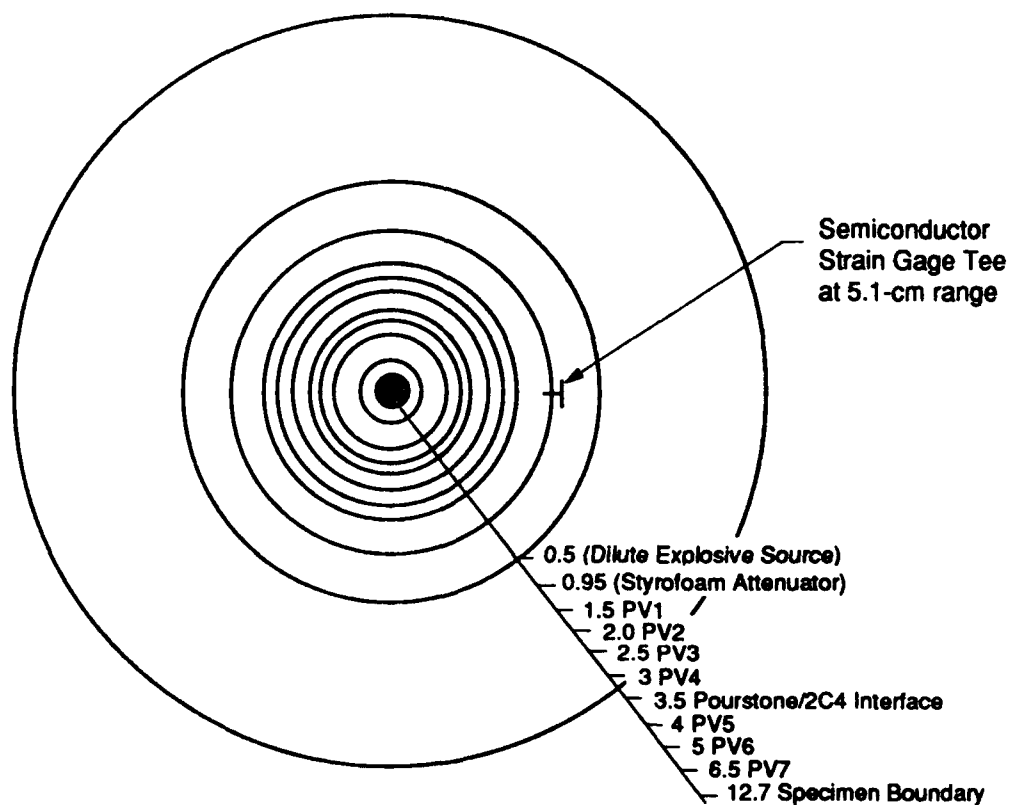
## 1.2 SOURCE EVALUATION EXPERIMENT

We conducted an experiment to characterize the source shown in Figure 2 and also to generate a velocity history to be used as a boundary condition for finite element code calculations of the surface wave experiments. A side view of the configuration for the source evaluation experiment is shown in Figure 3(a), and the top view is shown in Figure 3(b). In this experiment, the dilute explosive charge source was cast in a 7-cm plug of pourstone grout to mimic the source in the surface wave experiments and then cast in 2C4 grout. The resulting specimen was a cylinder 25.4-cm in diameter and 15 cm high. The center of the source was located 5.08 cm below the top of the specimen to match the surface wave experimental configuration. Copper loop particle velocity gages were cast in the specimen at radial distances of 1.5, 2.0, 2.5, and 3.0 cm in the pourstone, and at 4.0, 5.0, and 6.5 cm from the center of the source in the 2C4 grout. Semiconductor strain gages oriented in the principal directions were mounted to the top surface of the model at a radial distance from the axis of 5.1 cm to measure the radial and circumferential strain histories on the model surface.

To perform the experiment, the specimen is placed in a solenoid driven by a constant current power supply providing about 270 amps to the coil, generating a constant magnetic field of about 1800 gauss to the specimen. When the wave arrives at each gage position, the copper loop gage moves at the local particle velocity, generating a voltage



(a) Side view



(b) Top view

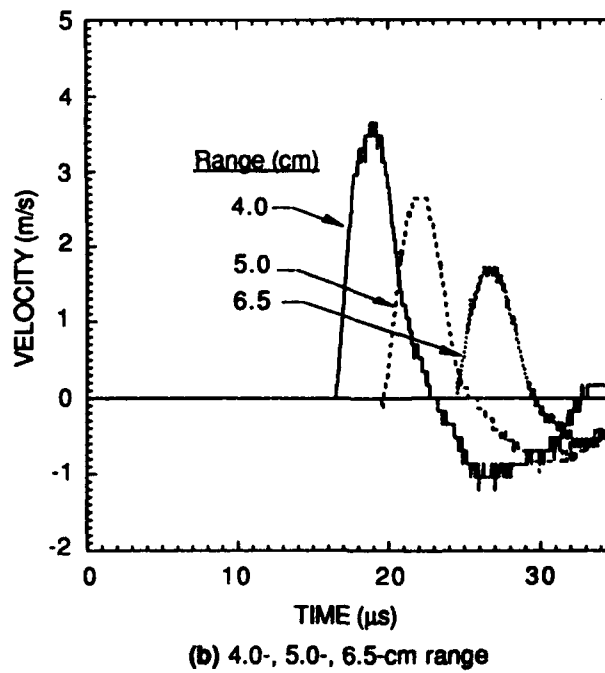
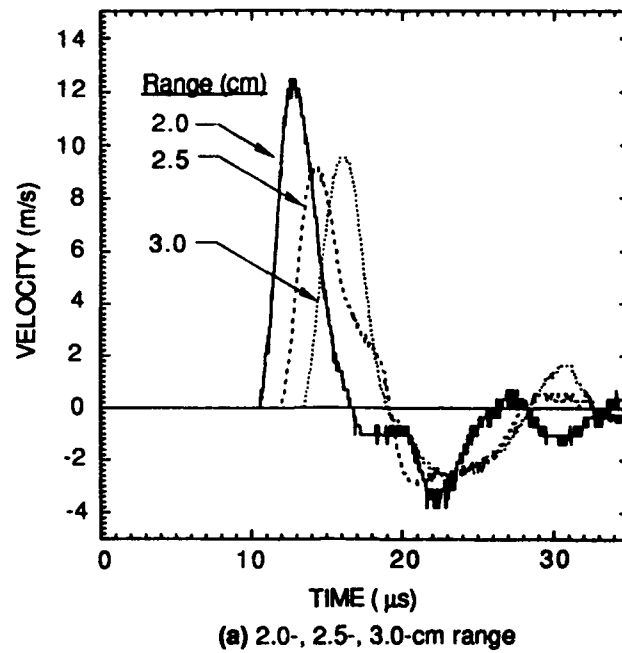
RM-7206-30

Figure 3. Configuration of source evaluation experiment.

proportional to the length of the conductor, the magnetic field strength, and the particle velocity. The experiment was performed at ambient pressure and room temperature.

The measured particle velocity histories from this experiment are shown in Figure 4. The radial particle velocity histories inside the pourstone grout plug are shown in Figure 4(a) at distances of 2.0, 2.5, and 3.0 cm from the center of the source, and the radial particle velocity histories in the 2C4 grout are shown in Figure 4(b) at the 4.0-, 5.0-, and 6.5-cm radii. Unfortunately, the oscilloscope overranged for the particle velocity gage at the 1.5-cm range, so the peak was not captured and the result is not presented. In Figure 4(a), we observe an outward pulse of about 8  $\mu$ s followed by about an 8- $\mu$ s negative phase. Some structure is observed in the record from reflections at the pourstone/2C4 interface, shown as a reduction in velocity at the 2-cm location around 21  $\mu$ s, and at the 2.5-cm location in the positive phase at around 18  $\mu$ s. The propagated pulse in the 2C4 grout [Figure 4(b)] is a smooth rise to the peak velocity and about a 7- $\mu$ s positive pulse duration, followed by a 10- $\mu$ s negative phase. The records are terminated when reflections from the top surface were approximated to arrive at each gage position. Reflections from the 2C4/pourstone interface were included in the finite element calculations, as all the structure in the waveform at the closer ranges was included in the imposed velocity boundary condition.

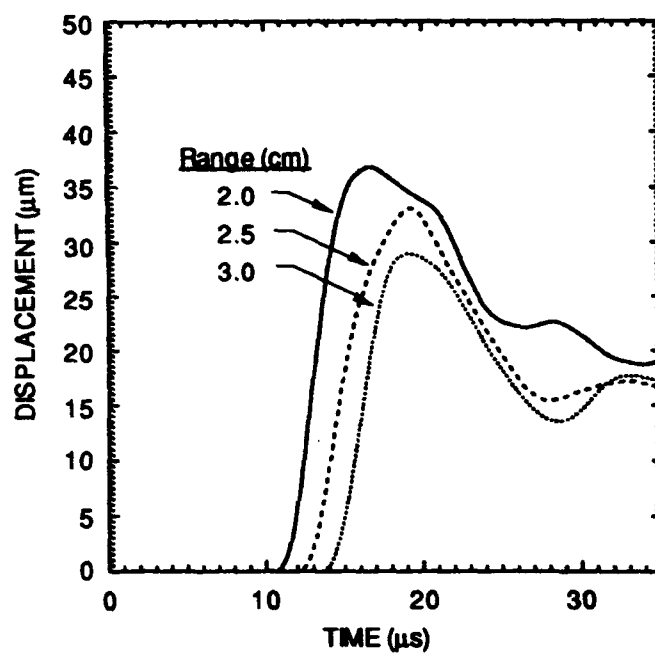
Displacements obtained by temporal integration of the velocity records are shown at the 2.0-, 2.5-, and 3.0-cm locations in Figure 5(a) and at the 4.0-, 5.0-, and 6.5-cm locations in Figure 5(b). Radial and circumferential strain histories measured at 5.1 cm from a cylindrical symmetry axis are shown in Figure 6.



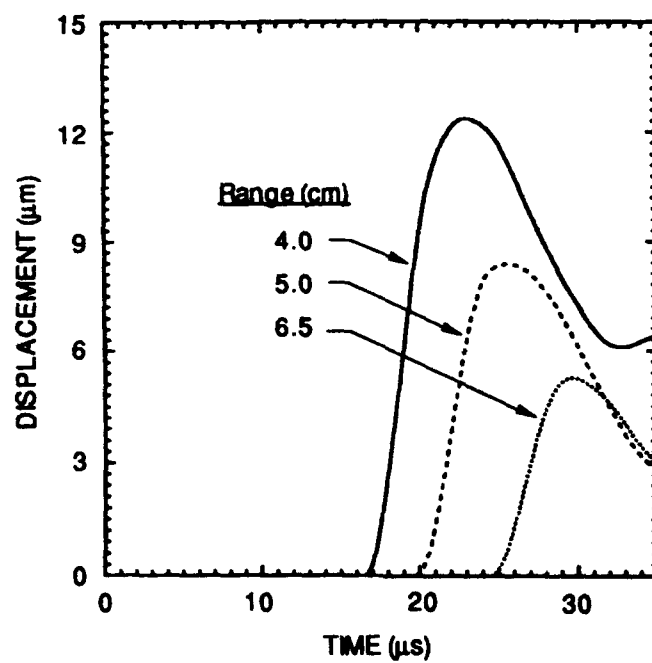
RAM-7206-31

Figure 4. Particle velocity histories measured in source evaluation experiment.





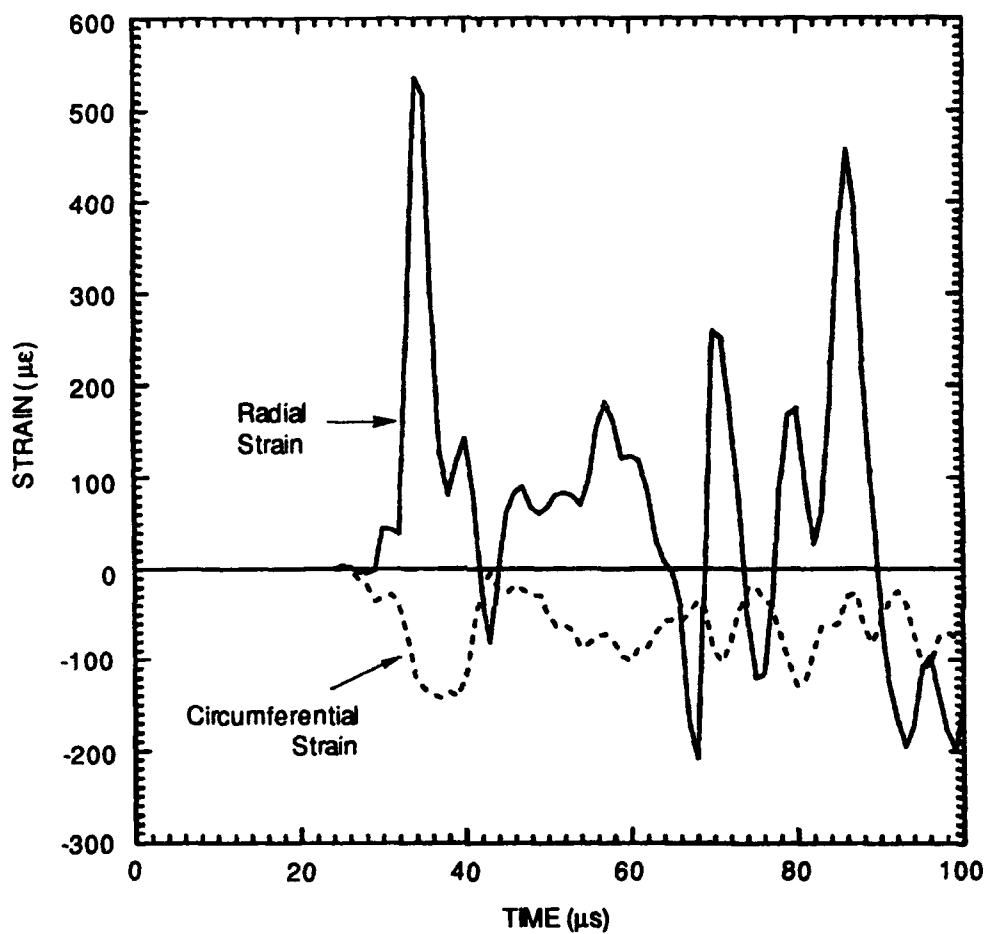
(a) 2.0-, 2.5-, 3.0-cm range



(b) 4.0-, 5.0-, 6.5-cm range

RAM-7206-32

Figure 5. Displacement histories measured in source evaluation experiment.



RAM-7206-33

Figure 6. Radial and circumferential surface strain histories measured in source evaluation experiment.

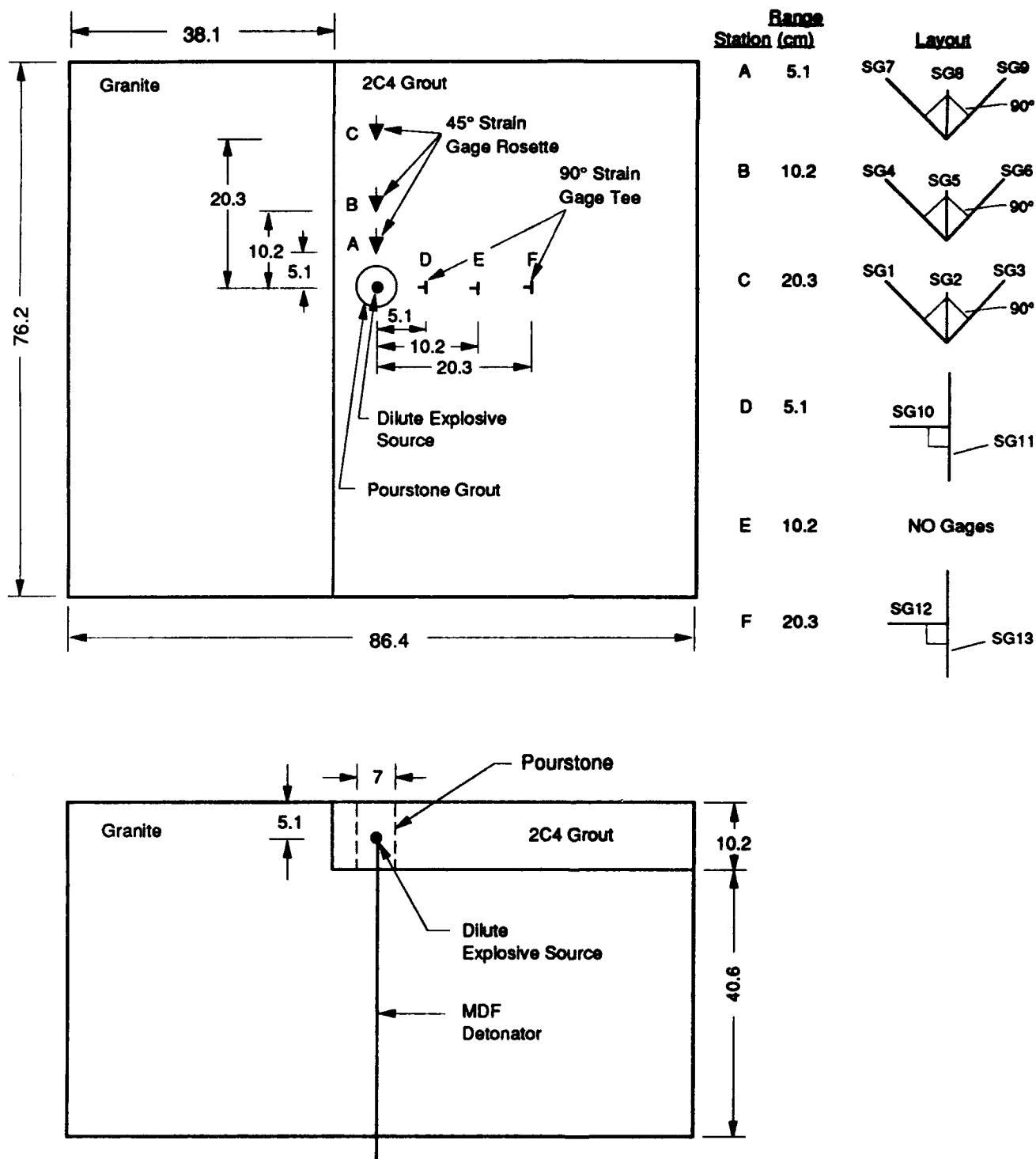
## **SECTION 2**

### **SURFACE WAVE EXPERIMENT AND CALCULATION**

The configuration for the surface wave experiments is shown in detail in Figure 7. In these experiments, a Sierra White granite block measuring 86.4 x 76.2 x 40.6 cm high served as the base onto which a 10.2-cm layer of 2C4 grout was cast. The scattering planar wall measured 38.1 x 76.2 x 10.2 cm and was bonded to the granite base using concrescive epoxy. Semiconductor strain gages were mounted on the surface of the 2C4 grout at three ranges parallel to the granite wall scattering surface and two ranges perpendicular to the wall. Parallel to the wall, 45-degree strain gage rosettes were located at 5.1 cm (Station A), 10.2 cm (Station B), and 20.3 cm (Station C) from the projection of the source onto the surface. In the direction perpendicular to the wall, strain gages forming a 90-degree tee configuration were mounted in the principal directions at 5.1 cm (Station D) and 20.3 cm (Station F). Station E refers to the 10.2-cm range perpendicular to the wall, but no gages were located at this position. The source was identical to that described previously. The strain gages were electronically calibrated prior to each experiment.

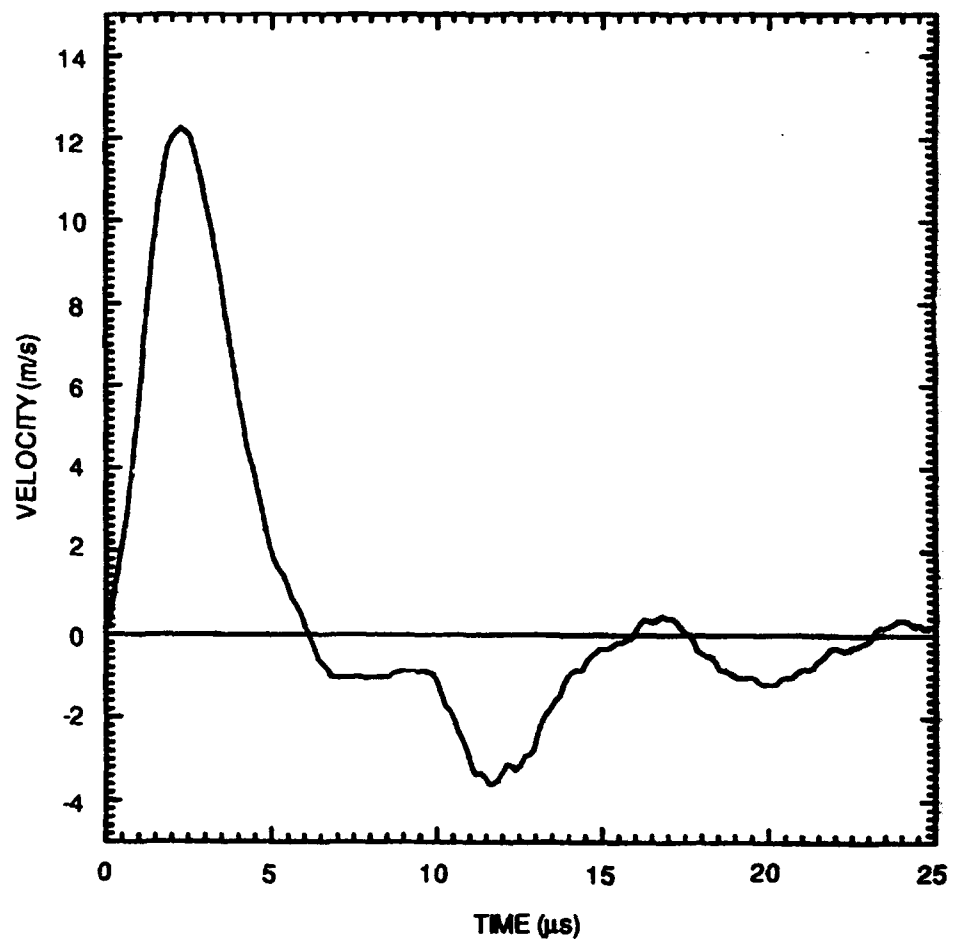
#### **2.1 FINITE ELEMENT CALCULATIONS**

Two finite element calculations were performed to analyze the formation of Love waves from a spherical (point) source. The calculations were performed with the finite element code DYNA3D. DYNA3D, developed at Lawrence Livermore National Laboratory,<sup>4</sup> is an explicit nonlinear three-dimensional finite element code for analyzing the dynamic response of solids and structures. The equations of motion are integrated in time using the central difference method. Spatial discretization was achieved with eight-node hexahedron (brick) elements. The material models used in our calculations are linear elastic models, and the material properties used for the granite and 2C4 grout are listed in Table 1. In the calculations, the 2C4 grout and pourstone assumed the same material properties. The load is applied by a spherical velocity boundary condition applied at a 2-cm-diameter location from the explosive source. The measured velocity time history shown in Figure 8 was used as the velocity condition in the calculations.



RM-7206-34

Figure 7. Gage layout and configuration of surface wave experiments.  
All dimensions in cm.



RAM-7206-35

Figure 8. Velocity boundary condition at 2-cm range input to finite element calculations.

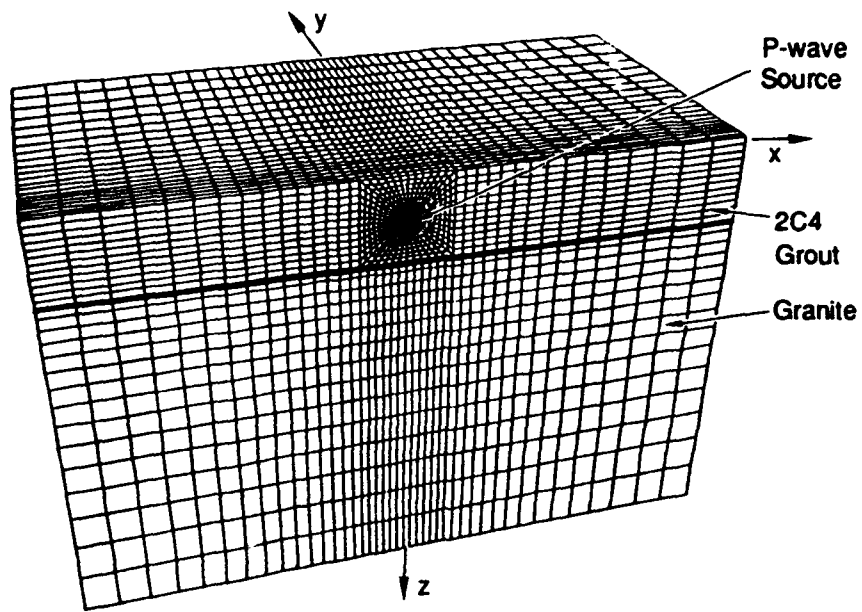
**Table 1****MATERIAL PROPERTIES USED IN FINITE ELEMENT CALCULATION**

	<u>Granite</u>	<u>2C4 Grout</u>	<u>Units</u>
$\rho$	2.7	1.8	grams/cm <sup>3</sup>
E	50.0	15.6	GPA
$\nu$	0.22	0.28	

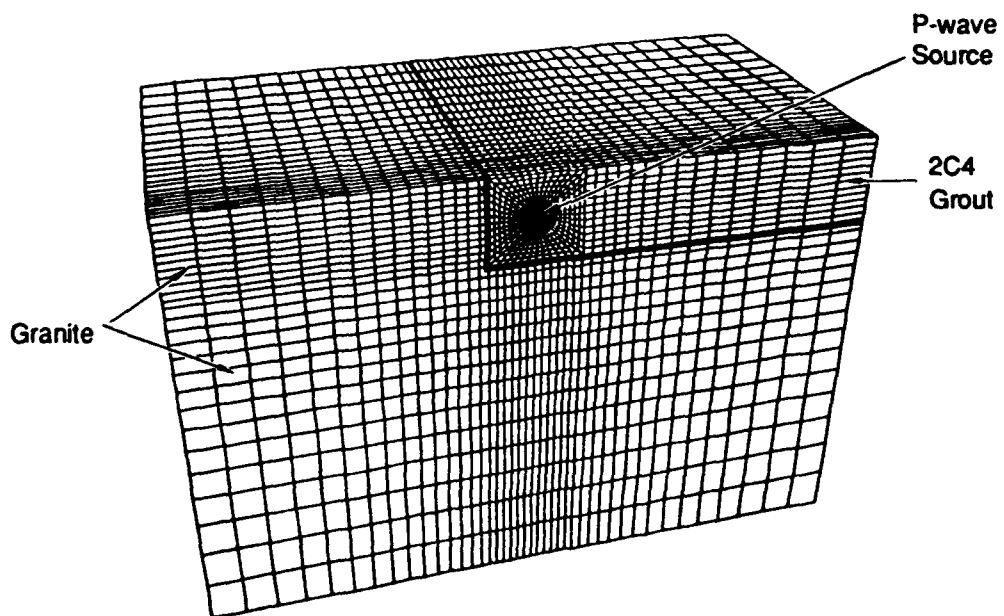
The meshes used in the calculations are shown in Figure 9. The meshes shown represent one half of the experimental configuration using a plane of symmetry passing through the spherical source. Figure 9(a) shows the first calculation representing a layer of grout over a granite half-space. Only one half of the mesh shown was actually used in the calculation using the additional symmetry plane that exists in the figure. The mesh used in this calculation contained a total of 12,771 elements. Figure 9(b) shows the second calculation representing a layer of grout over a granite half-space adjacent to a granite wall. The entire mesh shown was used in the calculation since no additional symmetry planes exist. The mesh used in this second calculation contained a total of 25,542 elements.

To illustrate the effect of the wall on the formation of the Love waves, the surface x-y shear strain fringes have been plotted at 50 and 75  $\mu$ s in Figures 10 and 11, respectively. Figures 10(a) and 11(a) show the first calculation (without the wall) for which the surface strains are dominated by a radially propagating P-wave. However, because the three-dimensional postprocessor plots Cartesian (x-y shear) strain components instead of a radial shear strain component, the regions of the figures near 45 degrees off of the principle x- and y-axes have an x-y shear component resulting from the local coordinate transformation from cylindrical to Cartesian reference frames. Along the principle x- and y-axes the calculation has no surface shear strain components as expected resulting from the radial symmetry of this problem.

For comparison, Figures 10(b) and 11(b) show the second calculation (with the wall) for which the surface strains along the x-axis are dominated by a radially propagating P-wave and the surface strains along the y-axis (parallel to the wall) show the development of the Love wave shearing strains. As described above, the shear strain components in the regions of the figures near 45 degrees off of the principal x- and y-axes are a result of the local coordinate transformation from cylindrical to Cartesian reference frames. Along the principle x-axis the calculation has no surface shear strain component as expected resulting



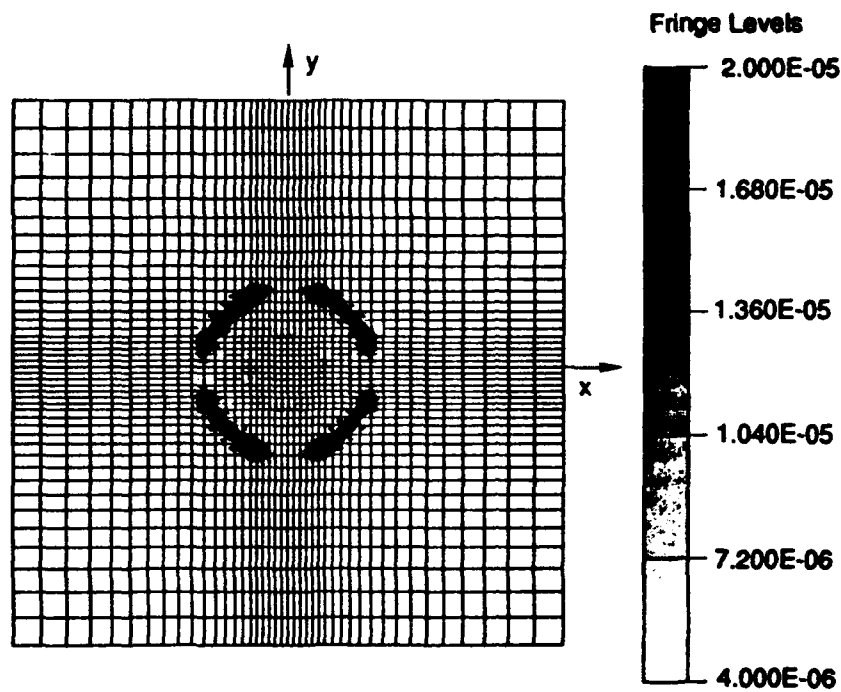
(a) Layer over half-space



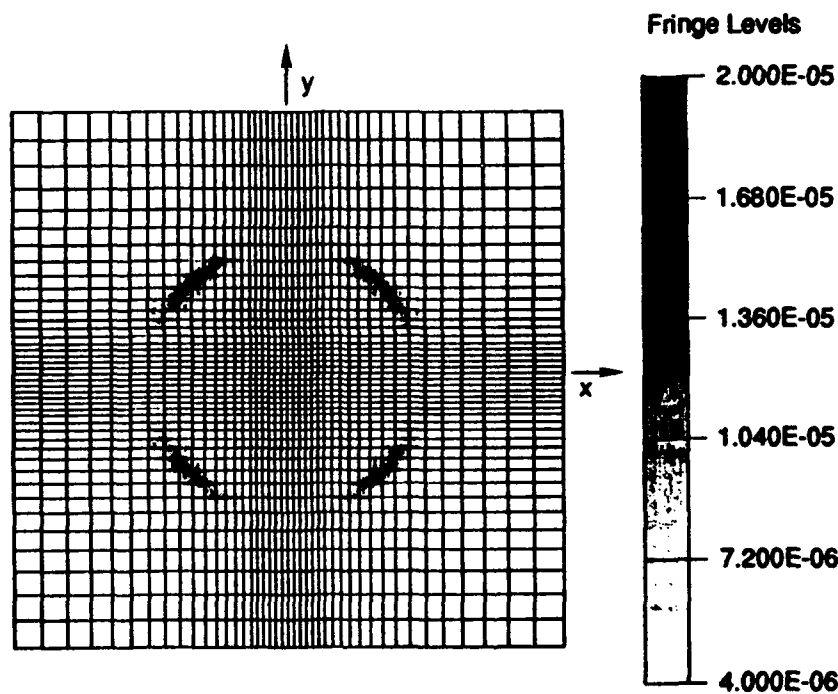
(b) Scatting wall

RA-7206-36

Figure 9. Finite element meshes.



(a)  $t = 50 \mu s$

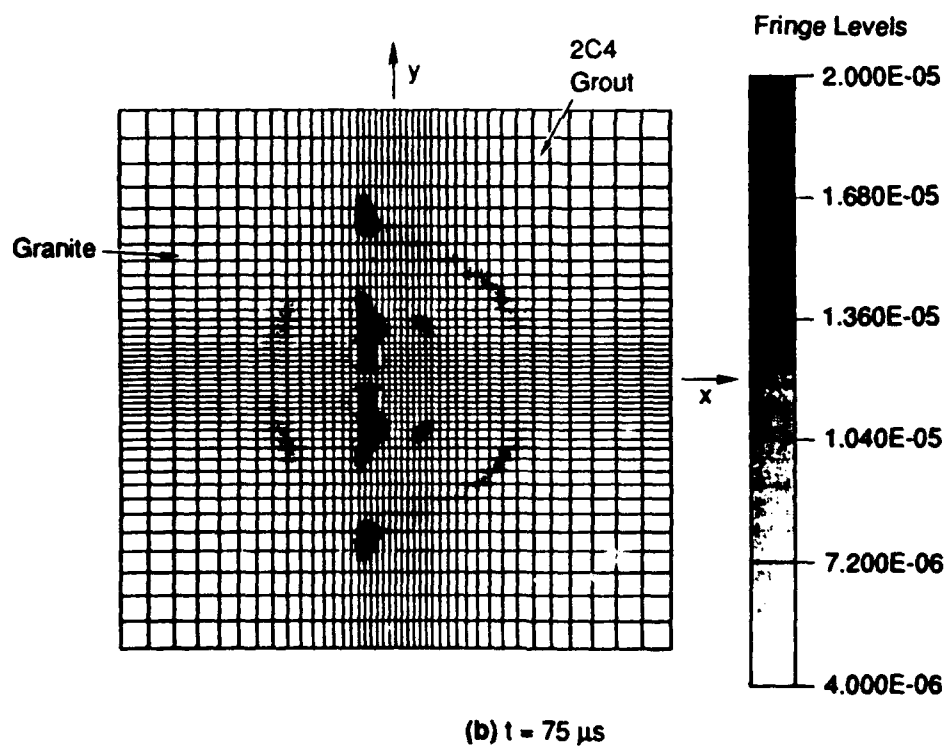
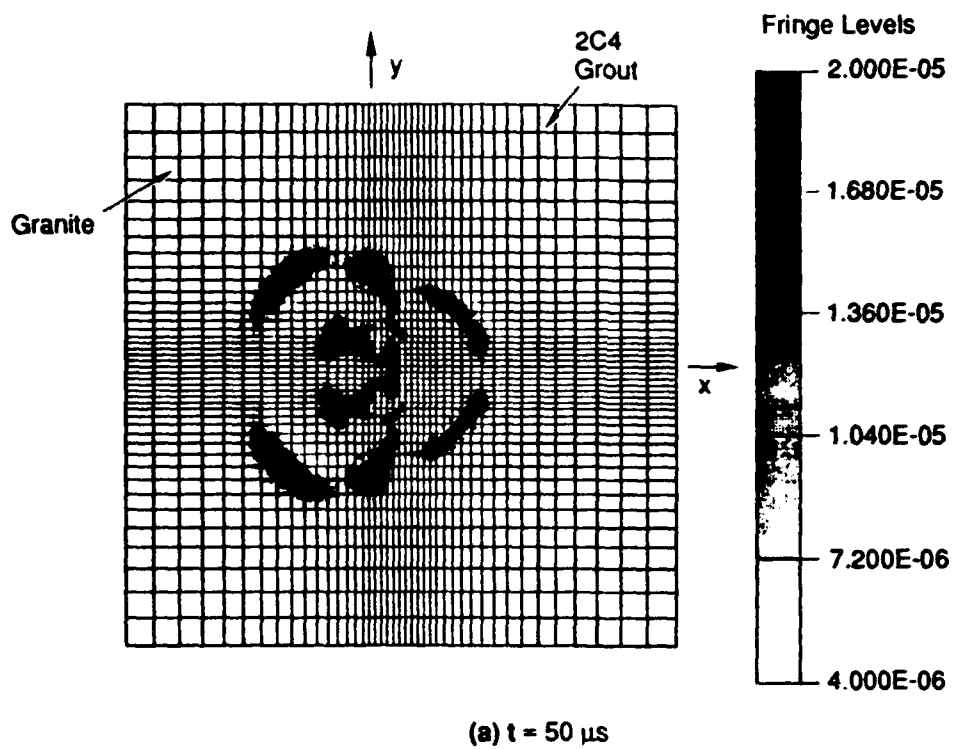


(b)  $t = 75 \mu s$

RA-7206-37

Figure 10. Top view of fringes of x-y surface shear strain for calculation without the wall (layer over half-space).





RA-7206-38

Figure 11. Top view of fringes of x-y surface shear strain in calculation with the wall.

from the symmetry of this problem about the x-z plane. However, along the y-axis adjacent to the wall the figure shows clearly the development of regions of significant shear strain, which along this axis represent the development of the Love wave shearing deformation. Figure 12 shows fringes of pressure for the case with the wall at 75  $\mu$ s.

The effect of the wall on propagation perpendicular to the wall is shown in the comparison of the two calculations at the 5.1- and 20.3-cm ranges (corresponding to Stations D and F) in (a) and (b), respectively, in Figure 13. Although minor differences in the x-x strain appear at the later times due to reflections off the wall, the effect is negligible and shows that this experimental geometry is appropriate for investigating both the layer-over-half-space and scattering surface cases.

## 2.2 COMPARISON OF EXPERIMENTS AND CALCULATION

In the calculation, time = 0 corresponds to the application of the velocity boundary condition at the 2-cm range. Therefore, we shifted the calculated times 10.5  $\mu$ s to correspond with the actual time in the experiment. The results from the surface wave experiments are shown superposed with the results from code calculations at each station on the surface in Figures 14 through 18. The record for each gage position (identified by Stations A-F) is shown as an average of three experiments. The data from the experiments used in the averaging is shown in the Appendix and demonstrates excellent repeatability, particularly at the farther ranges. One gage each at the 5.08-cm (SG9) and 20.3-cm (SG2) locations along the direction of the wall failed prior to the experiments and no data was recovered at these measurement positions. In all figures, compression is positive in our sign convention.

Figure 14 shows the comparison of experiment and calculation at Station A, located at the 5.1-cm range parallel to the scattering surface. The calculated results were transformed to correspond to the strain measured by the strain gage. The data shows an initial positive pulse from the direct P-wave, followed by a large amplitude negative phase from the free-surface reflected tension. At later times, the calculation shows low-amplitude oscillations around zero in the y-y strain direction, and a low-amplitude final tensile condition in the direction rotated 45 degrees from the y-axis. Overall, the data obtained from the strain gages captures the basic features of the waveform, although the experimental data shows slightly larger amplitude strains than those calculated. Moving out to the farther ranges at Station B (10.2 cm) and Station C (20.3 cm), shown in Figures 15 and 16, respectively, the calculated and measured strains show very good agreement in the

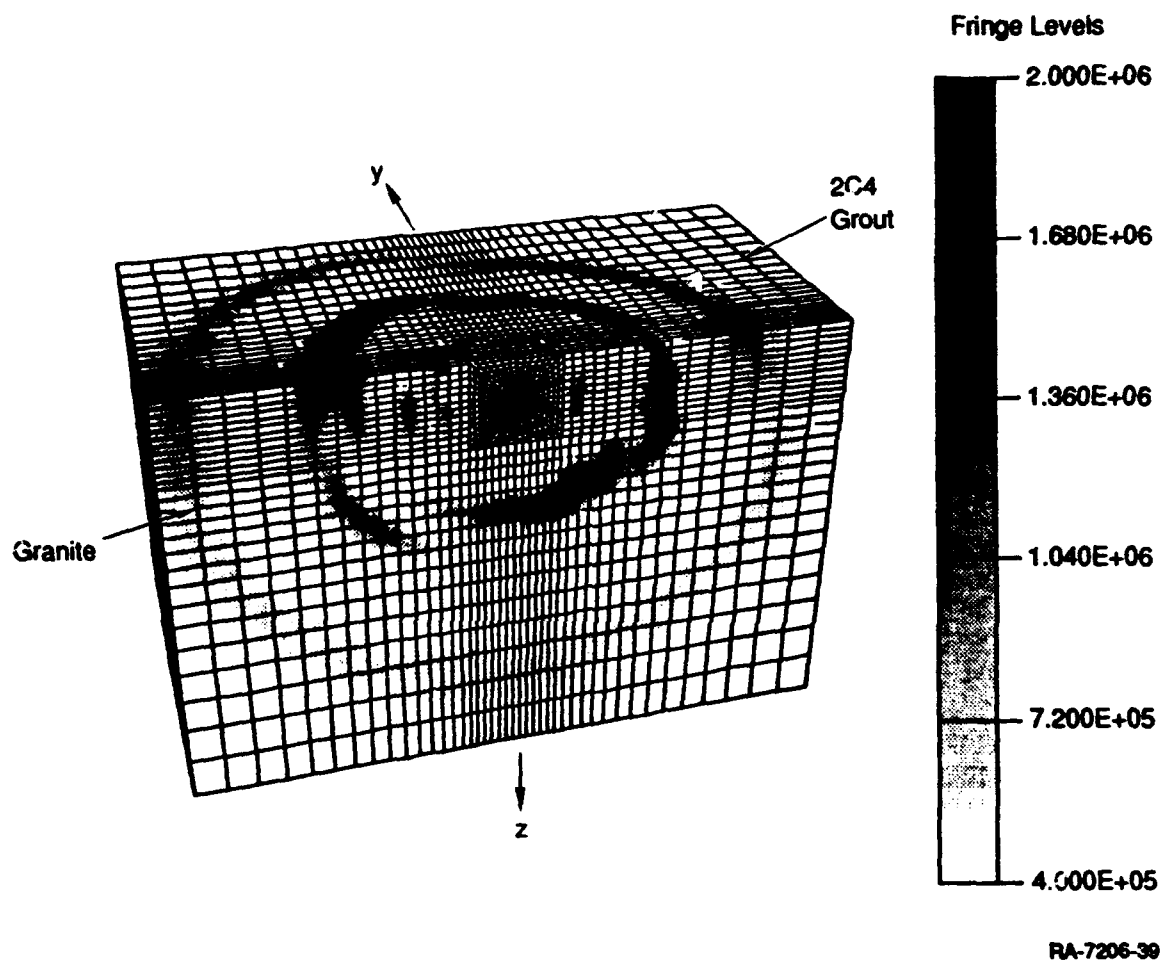
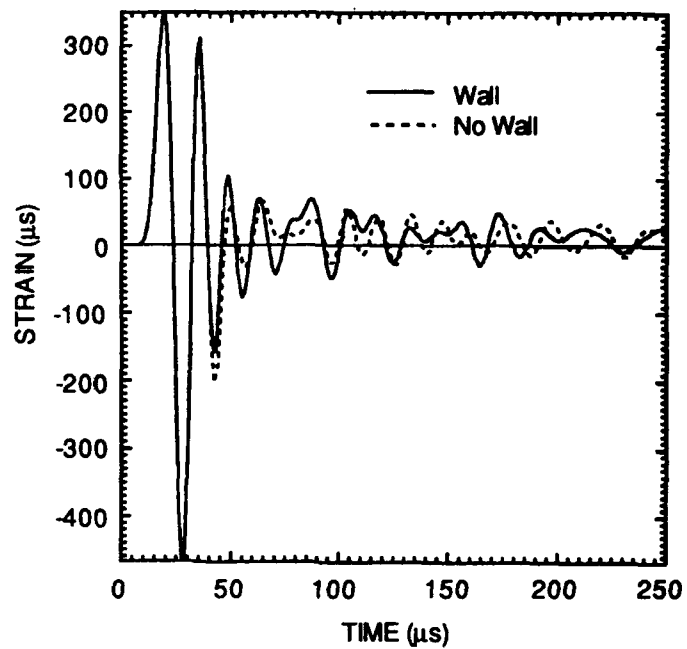
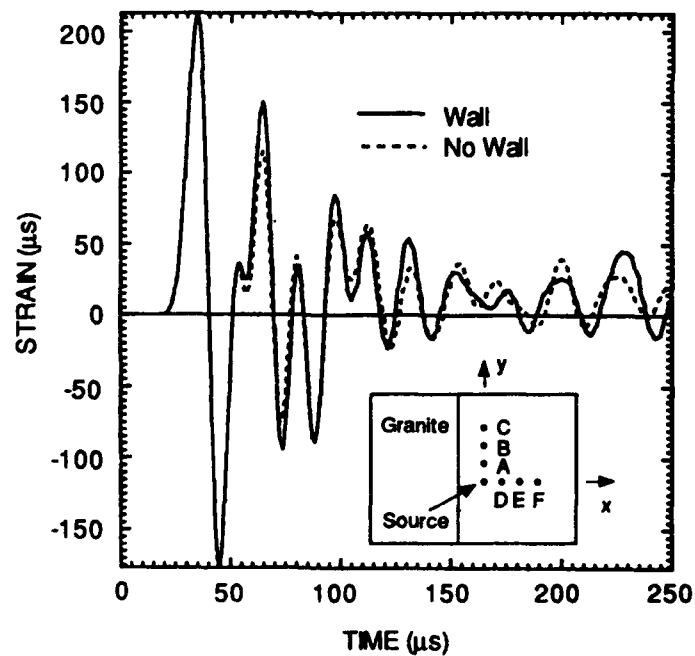


Figure 12. Fringes of pressure at  $75 \mu s$  for calculation with the wall.



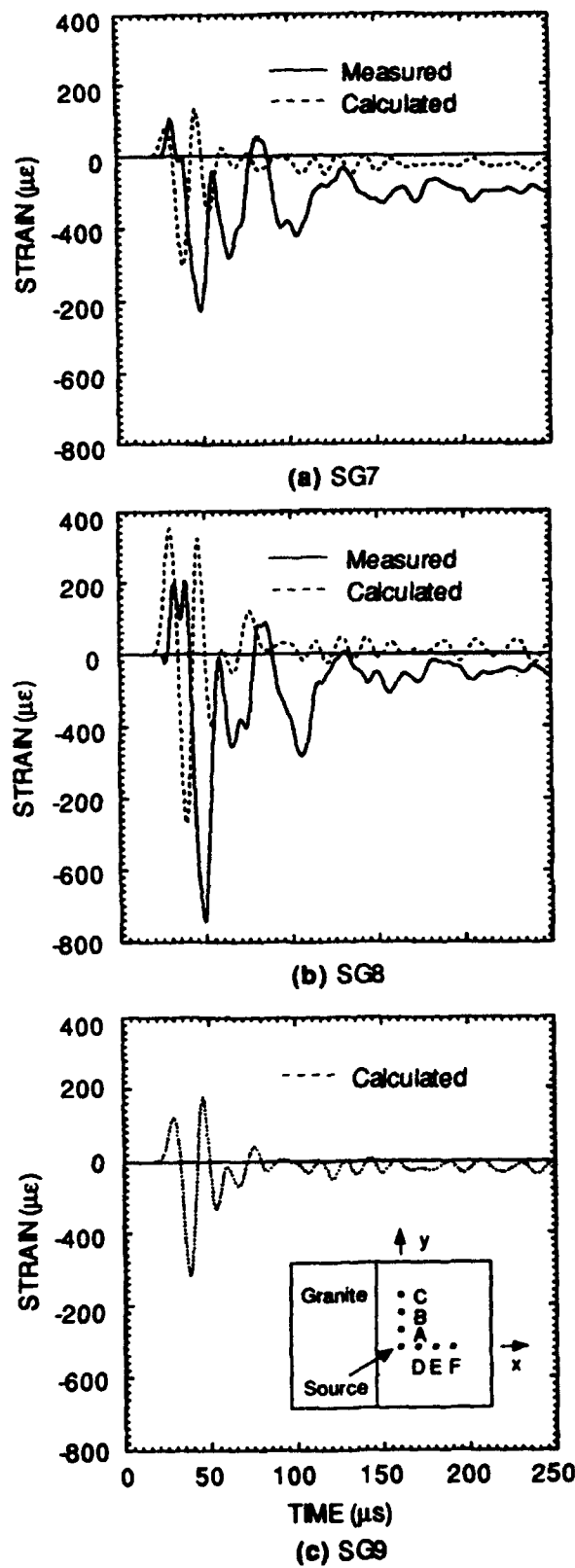
(a) 5.08-cm range (Station D)



(b) 20.3-cm range (Station F)

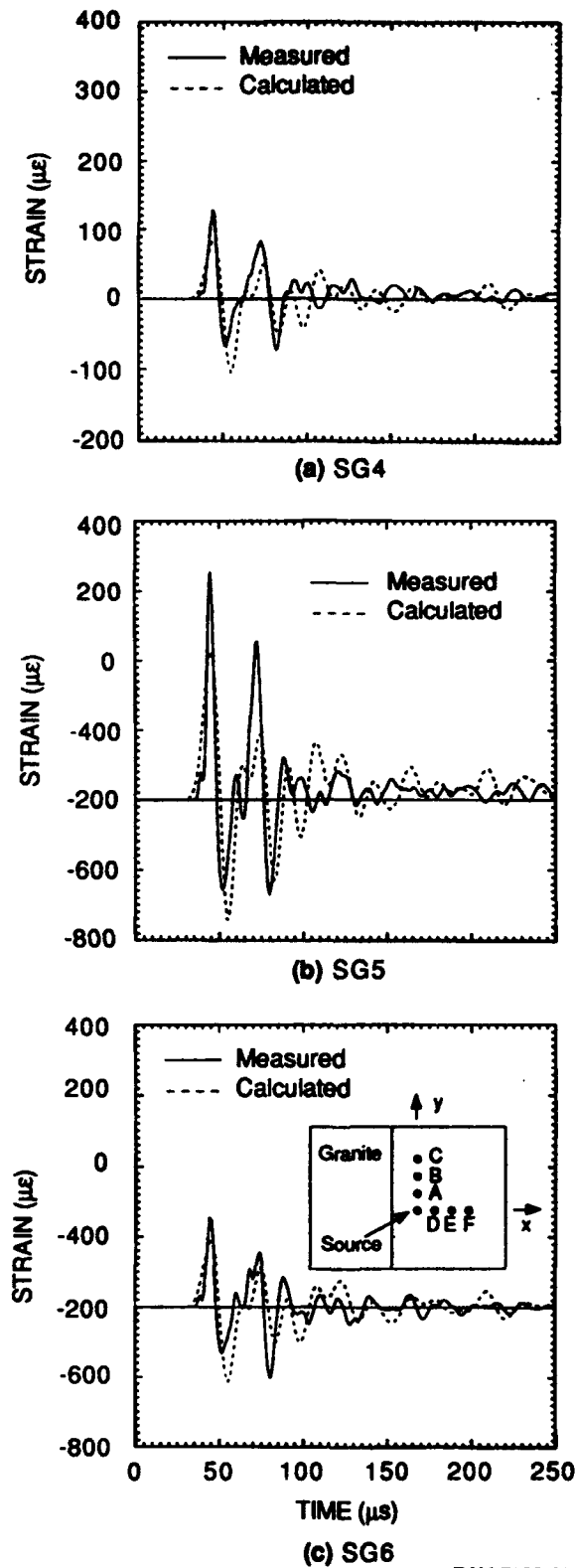
RAM-7206-40

Figure 13. Effect of wall on strain in direction perpendicular to wall.



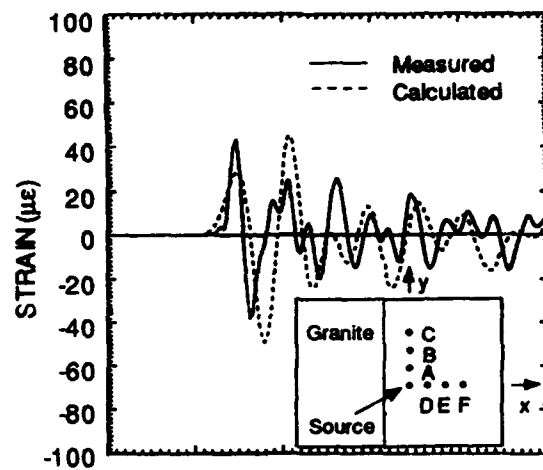
RAM-7208-41

Figure 14. Measured and calculated surface strain histories at Station A (5.1-cm range parallel to wall) in surface wave experiments.

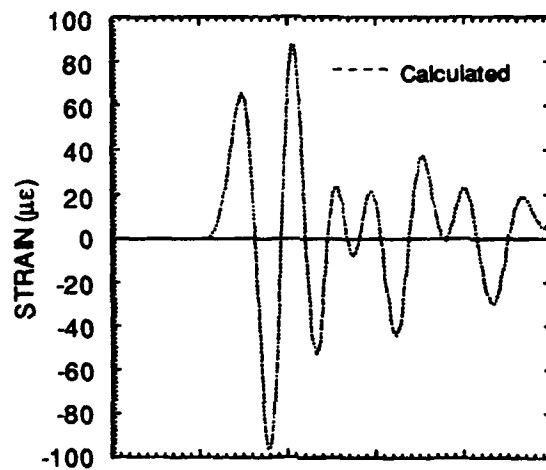


RAM-7208-42

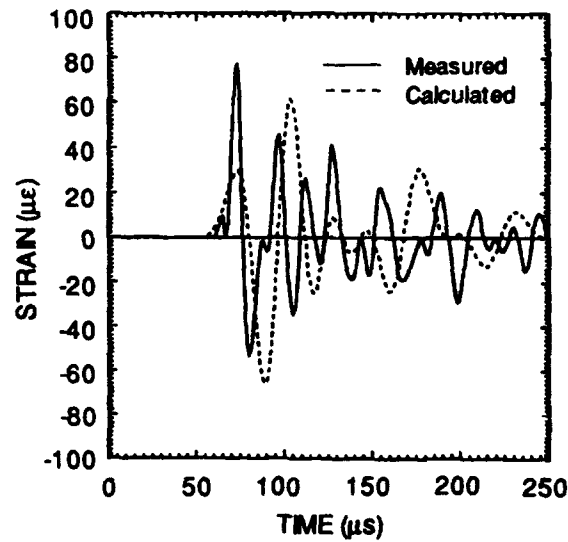
Figure 15. Measured and calculated surface strain histories at Station B (10.2-cm range parallel to wall) in surface wave experiments.



(a) SG1



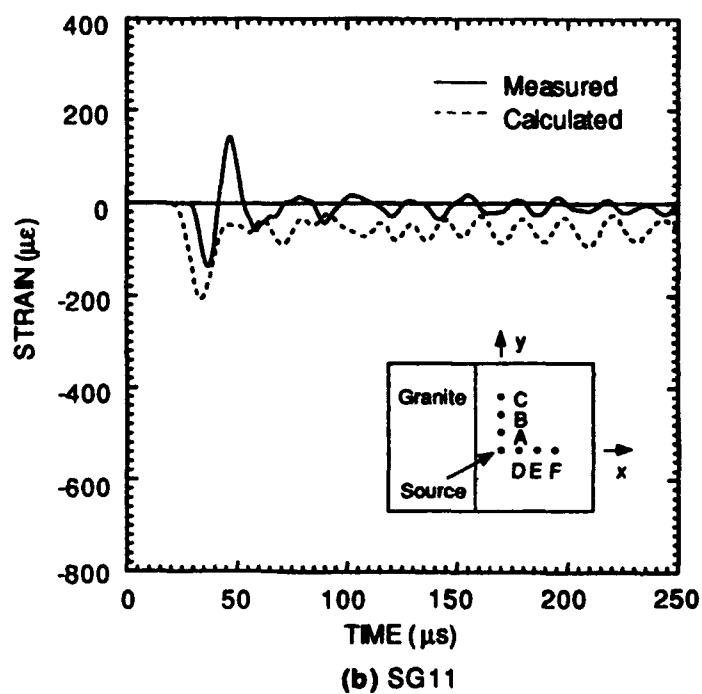
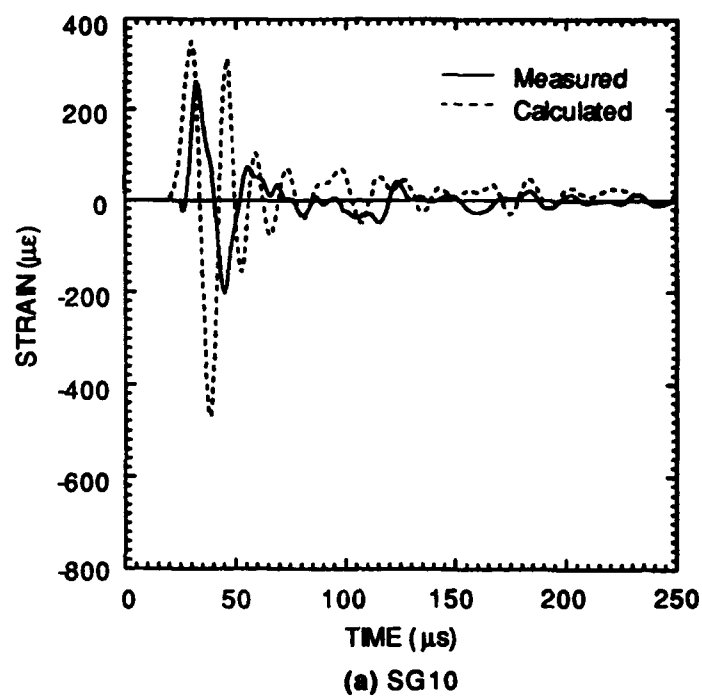
(b) SG2



(c) SG3

RA-7206-43

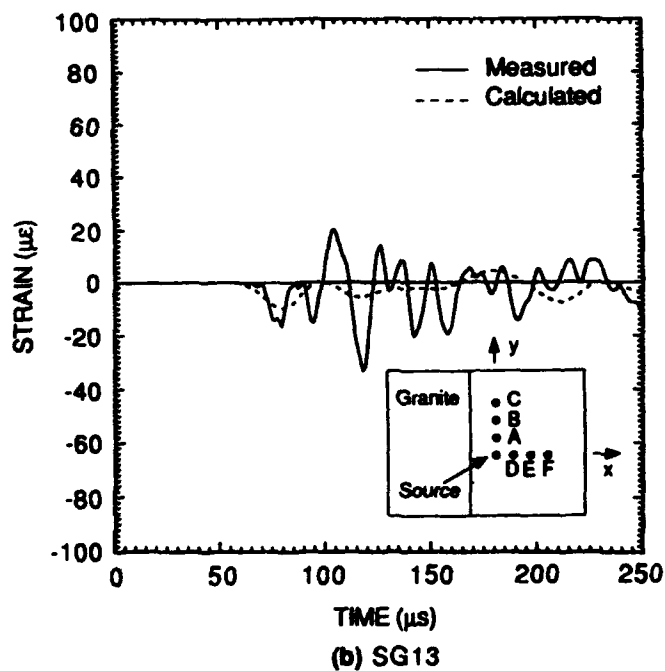
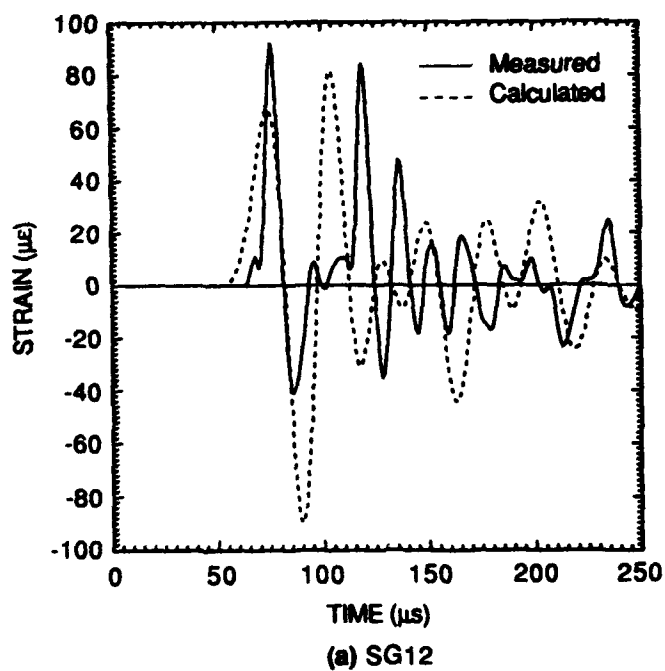
Figure 16. Measured and calculated surface strain histories at Station C (20.3-cm range parallel to wall) in surface wave experiments.



RAM-7206-44

Figure 17. Measured and calculated surface strain histories at Station D (5.1-cm range perpendicular to wall) in surface wave experiments.





RAM-7208-45

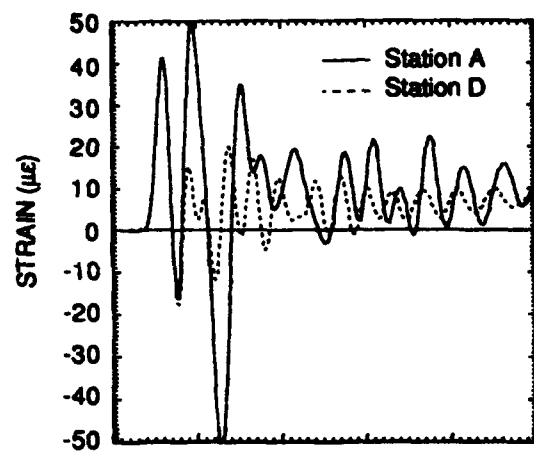
Figure 18. Measured and calculated surface strain histories at Station F (20.3-cm range perpendicular to wall) in surface wave experiments.

general character of the waveform, although the measured amplitude is a bit higher than calculated. Nevertheless, most of the prominent features are observed.

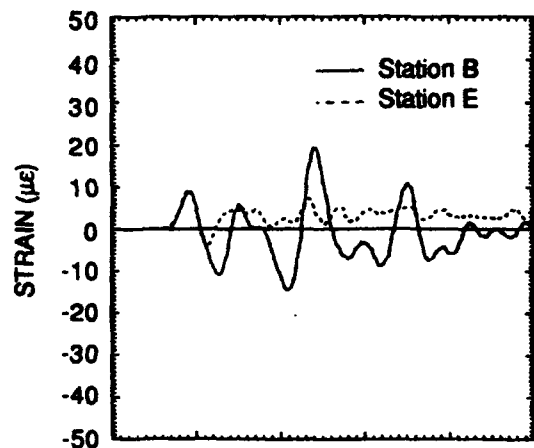
The data is shown superposed on the calculated results at Stations D and E in Figures 17 and 18, respectively. In the direction perpendicular to the wall, the gages were oriented at 90 degrees corresponding to the principal strain directions. In Figure 17(a) (Station D at 5.1 cm), the data and calculation show an initial compressional pulse in the radial direction from the direct P-wave, followed by a large-amplitude tensile pulse. The general feature at this location is a large-amplitude initial pulse followed by very low-amplitude oscillations about zero in the radial direction, and a negative tensile strain in circumferential direction [Figure 17(b)]. The observed time difference is a computational artifact due to the position within the element where strain is calculated. At the 20-cm location (Station F), the data and calculation show some late-time oscillations of similar amplitude to the initial pulse and are most likely the result of surface waves propagating within the waveguide layer. Overall, we are pleased with agreement between experiment and theory, particularly because of the extremely low-amplitude signals measured and the excellent repeatability shown in the Appendix. Because the code has been satisfactorily validated by experiment, we can use the code results to analyze the propagation of Love waves within the surface.

Figure 19 shows a comparison of the x-y shear strain (Love wave component) at stations parallel and perpendicular to the wall. Stations A and D are shown superposed in Figure 19(a), Stations B and E in Figure 19(b), and Stations C and F in Figure 19(c). The horizontal shear deformation perpendicular to the wall is an artifact of the calculation because the element was not centrally located along the symmetry plane. Nevertheless, we can subtract one result from the other because this artifact is inherent in both directions.

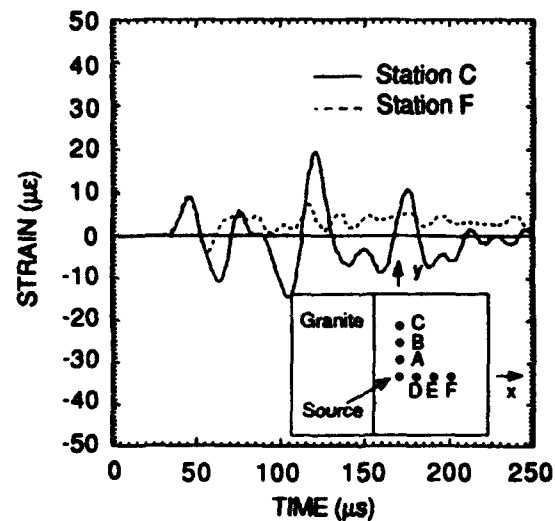
The differences in x-y shear strain in the two directions on the surface are the Love waves, and the propagation of the Love waves is shown in Figure 20(a) through (c). At the 5.1-cm range, the x-y shear strain is observed to consist of fairly high-frequency (~100 kHz) oscillations, maintaining an amplitude of about 20  $\mu\epsilon$  at the later times. As the Love wave propagates to the further ranges, shown in Figure 20(a) and (b), the amplitude remains at about 20  $\mu\epsilon$ , but the period has increased and most high frequencies have disappeared. An interesting feature is that the polarity switches from positive shear to negative shear with propagation. These results show that a planar wall can contribute a significant Love wave component to the signal despite the purely compressional source.



(a) Station A and D (5.1-cm range)



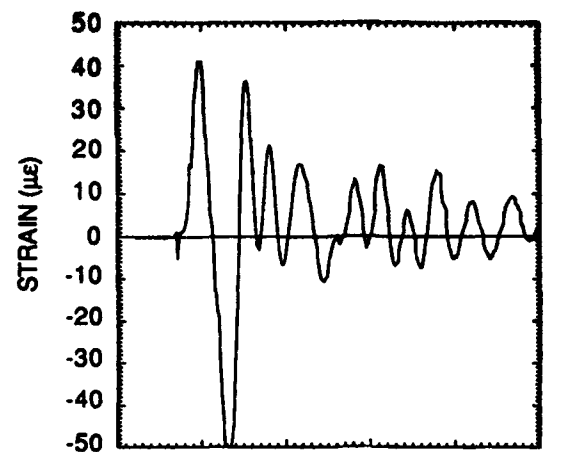
(b) Station B and E (10.2-cm range)



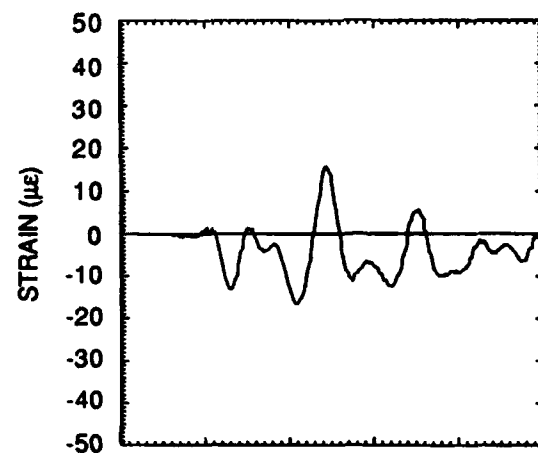
(c) Station C and F (20.3-cm range)

RAM-7206-46

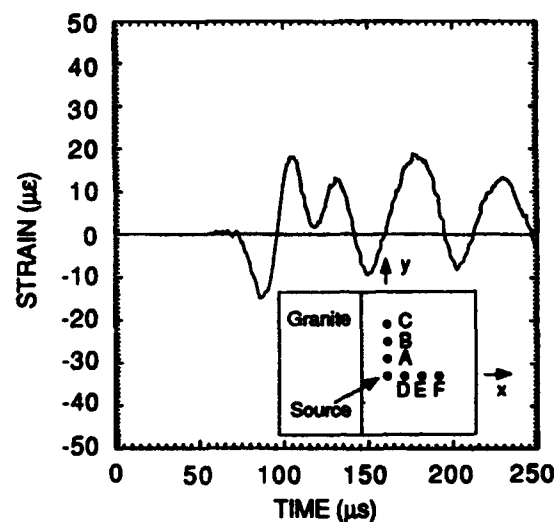
Figure 19. Comparison of calculated x-y shear strain parallel and perpendicular to wall.



(a) Station A



(b) Station B



(c) Station C

RAM-7208-47

Figure 20. Calculated Love waves at Stations A, B, and C.

### **SECTION 3**

### **CONCLUSIONS**

We have presented experimental results that show good agreement with finite element calculations of this experimental geometry. At each location, test repeatability was also good and the data were adequate to validate the code. The results from the code show the formation of a Love wave component generated by the shear tractions at the interface of the two materials, and show that this component is propagated with little dissipation to the further ranges. The results show a blending of the high-frequency component of the Love waves into lower-frequency packets with propagation. This result is not unexpected; however, it is encouraging that this experimental technique can provide high-quality data from a low-energy source to validate codes for investigating Love wave propagation in more complex geometries.

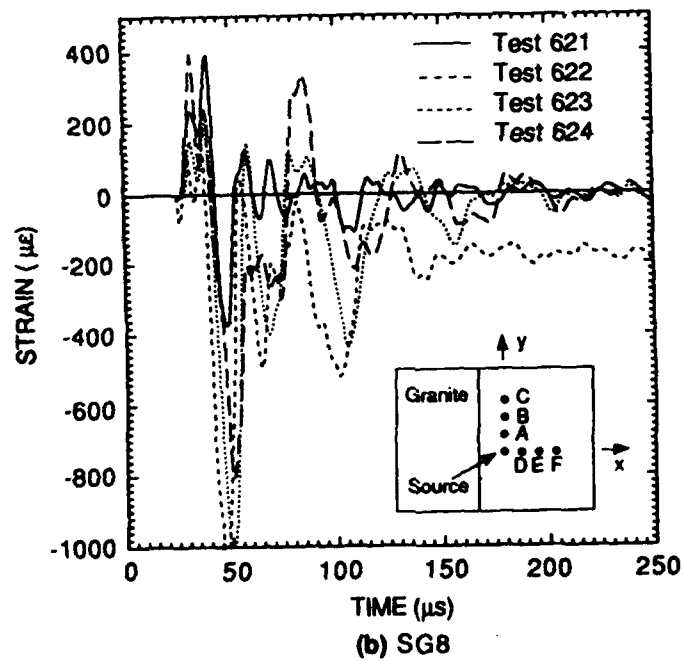
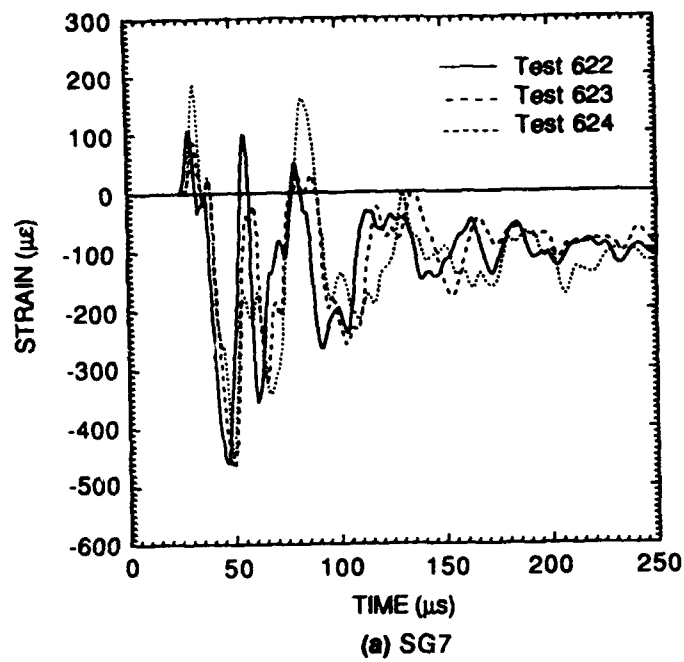
## SECTION 4

### REFERENCES

1. Miller, S. A., and A. L. Florence, "Formation and Propagation of Love Waves from a P-wave Source," Final Report, Geophysics Laboratory, Contract GL-TR-90-0100 (1990), ADA225559.
2. Miller, S. A., and A. L. Florence, "Laboratory Particle Velocity Experiments on Indiana Limestone and Sierra White Granite," Final Report, Geophysics Laboratory, Contract F19628-91-K-0003 (1991), PL-TR-91-2277. ADA248045
3. Dobratz, B. M., *Explosives Handbook* (Properties of Chemical Explosives and Explosive Simulants), Lawrence Livermore National Laboratory Report DE85-015961 (March 16, 1981).
4. Hallquist, J. O., and R. G. Whirley, 1989, *DYNA3D User's Manual* (Nonlinear Dynamic Analysis of Structures in Three Dimensions), Lawrence Livermore National Laboratory Report, Rev. 2.

## **APPENDIX A**

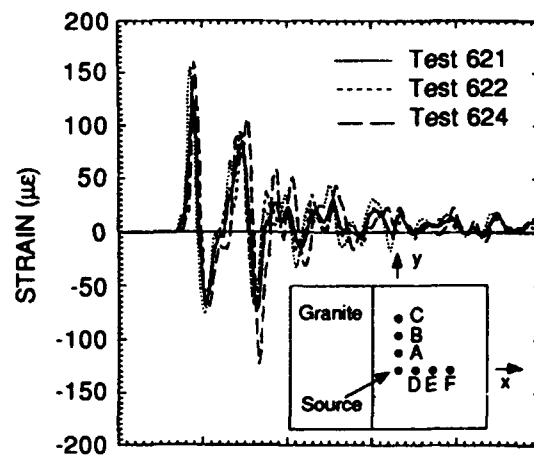
The results from three experiments are shown superposed at each gage position in Figures A.1 through A.5 to demonstrate repeatability between tests.



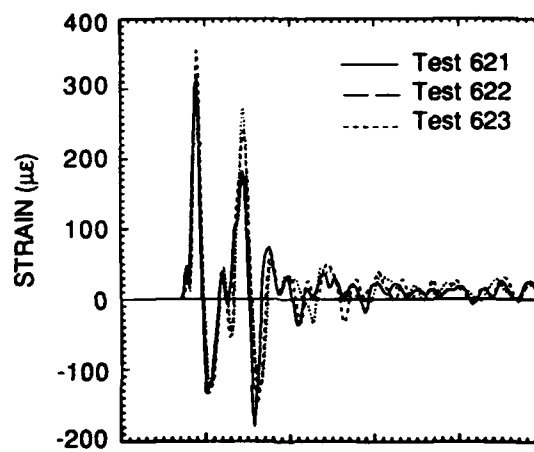
RAM-7206-48

Figure A.1. Measured surface strain histories at Station A (5.1-cm range parallel to wall) in surface wave experiments.

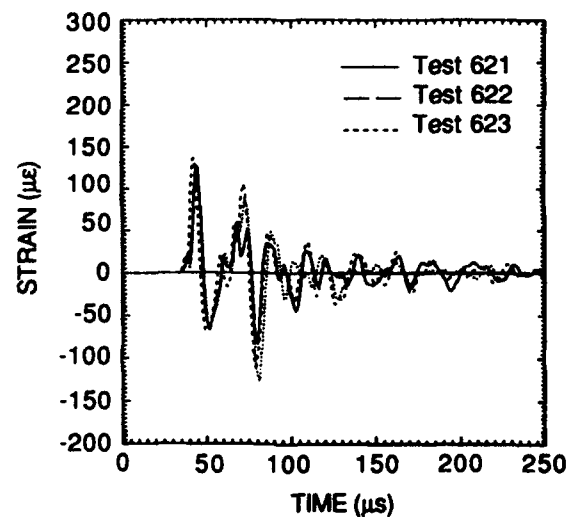




(a) SG4



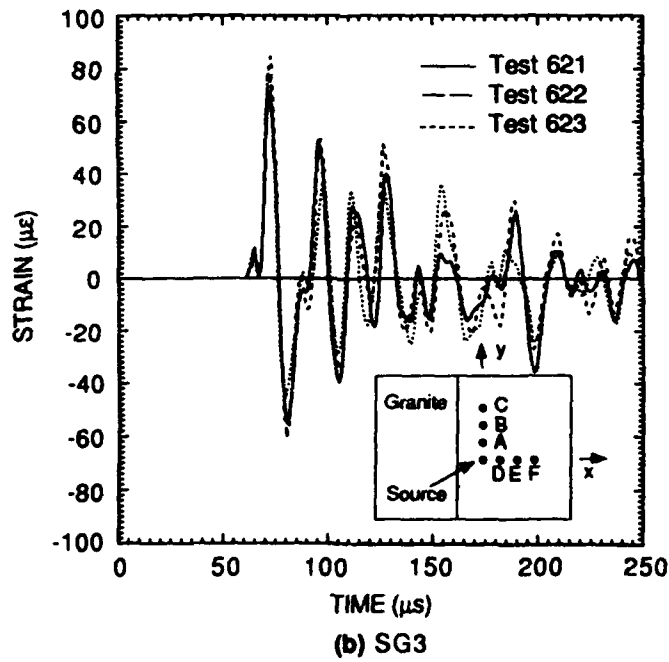
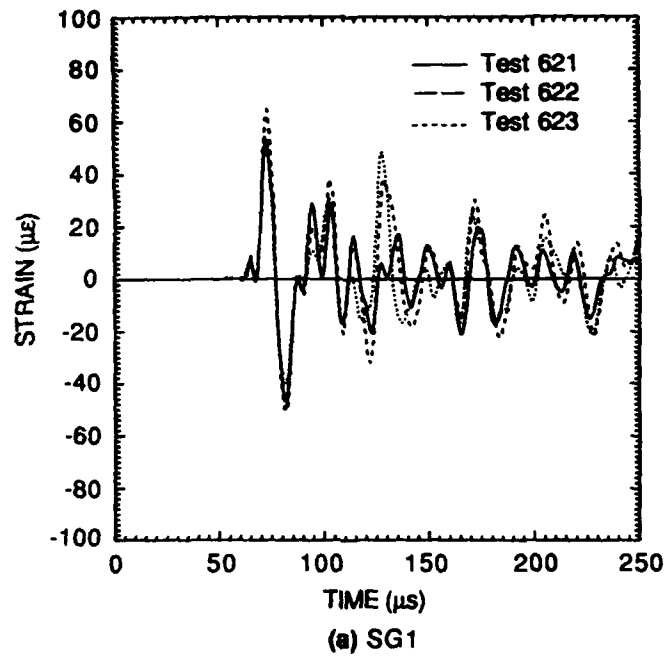
(b) SG5



(c) SG6

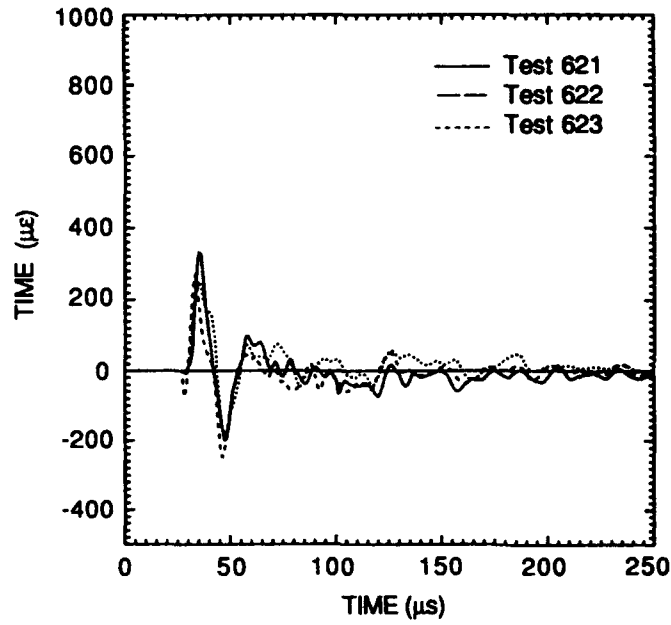
RAM-7206-49

Figure A.2. Measured surface strain histories at Station B (10.2-cm parallel to wall) in surface wave experiments.

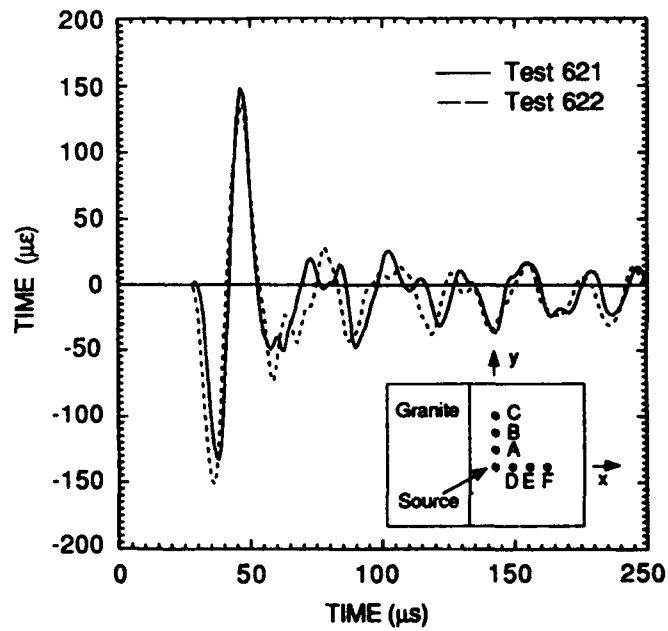


RAM-7206-50

Figure A.3. Measured surface strain histories at Station C (20.3-cm range parallel to wall) in surface wave experiments.



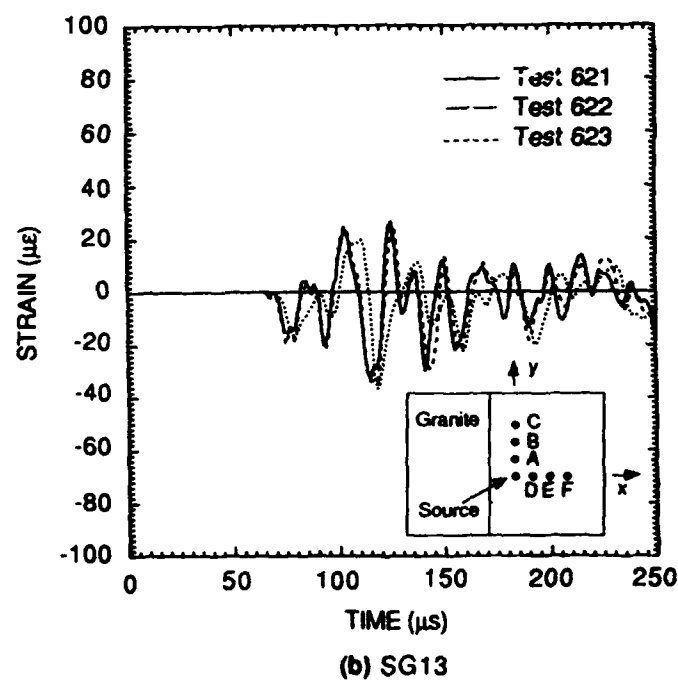
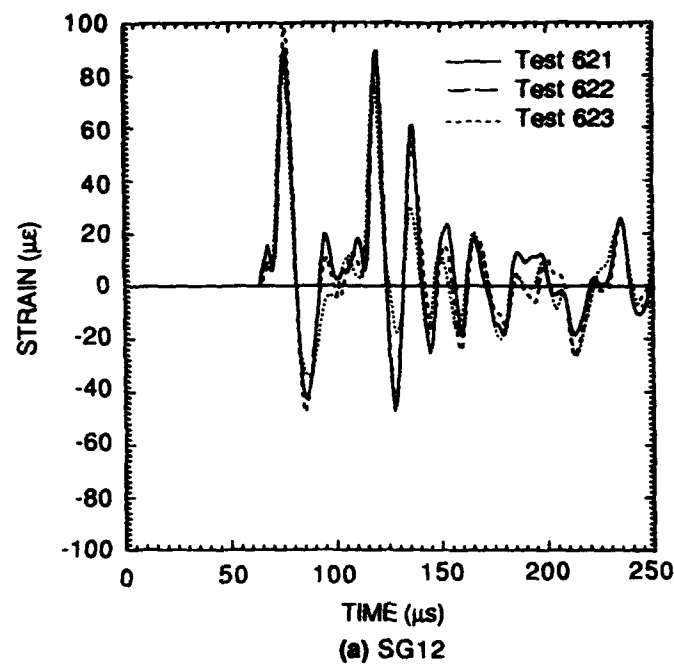
(a) SG10



(b) SG11

RAM-7208-51

Figure A.4. Measured surface strain histories at Station D (5.1-cm range perpendicular to wall) in surface wave experiments.



RAM-7206-52

Figure A.5. Measured surface strain histories at Station F (20.3-cm range perpendicular to wall) in surface wave experiments.

Prof. Thomas Ahrens  
Seismological Lab, 252-21  
Division of Geological & Planetary Sciences  
California Institute of Technology  
Pasadena, CA 91125

• Prof. Keiiti Aki  
Center for Earth Sciences  
University of Southern California  
University Park  
Los Angeles, CA 90089-0741

Prof. Shelton Alexander  
Geosciences Department  
403 Deike Building  
The Pennsylvania State University  
University Park, PA 16802

Dr. Ralph Alewine, III  
DARPA/NMRO  
3701 North Fairfax Drive  
Arlington, VA 22203-1714

Prof. Charles B. Archambeau  
CIRES  
University of Colorado  
Boulder, CO 80309

Dr. Thomas C. Bache, Jr.  
Science Applications Int'l Corp.  
10260 Campus Point Drive  
San Diego, CA 92121 (2 copies)

Prof. Muawia Barazangi  
Institute for the Study of the Continent  
Cornell University  
Ithaca, NY 14853

Dr. Jeff Barker  
Department of Geological Sciences  
State University of New York  
at Binghamton  
Vestal, NY 13901

• Dr. Douglas R. Baumgardt  
• ENSCO, Inc  
5400 Port Royal Road  
Springfield, VA 22151-2388

Dr. Susan Beck  
Department of Geosciences  
Building #77  
University of Arizona  
Tucson, AZ 85721

Dr. T.J. Bennett  
S-CUBED  
A Division of Maxwell Laboratories  
11800 Sunrise Valley Drive, Suite 1212  
Reston, VA 22091

Dr. Robert Blandford  
AFTAC/TT, Center for Seismic Studies  
1300 North 17th Street  
Suite 1450  
Arlington, VA 22209-2308

Dr. G.A. Bollinger  
Department of Geological Sciences  
Virginia Polytechnical Institute  
21044 Derring Hall  
Blacksburg, VA 24061

Dr. Stephen Bratt  
Center for Seismic Studies  
1300 North 17th Street  
Suite 1450  
Arlington, VA 22209-2308

Dr. Lawrence Burdick  
Woodward-Clyde Consultants  
566 El Dorado Street  
Pasadena, CA 91109-3245

Dr. Robert Burrige  
Schlumberger-Doll Research Center  
Old Quarry Road  
Ridgefield, CT 06877

Dr. Jerry Carter  
Center for Seismic Studies  
1300 North 17th Street  
Suite 1450  
Arlington, VA 22209-2308

Dr. Eric Chael  
Division 9241  
Sandia Laboratory  
Albuquerque, NM 87185

Prof. Vernon F. Cormier  
Department of Geology & Geophysics  
U-45, Room 207  
University of Connecticut  
Storrs, CT 06268

Prof. Steven Day  
Department of Geological Sciences  
San Diego State University  
San Diego, CA 92182

Marvin Denny  
U.S. Department of Energy  
Office of Arms Control  
Washington, DC 20585

Dr. Cliff Frolich  
Institute of Geophysics  
8701 North Mopac  
Austin, TX 78759

Dr. Zoltan Der  
ENSCO, Inc.  
5400 Port Royal Road  
Springfield, VA 22151-2388

Dr. Holly Given  
IGPP, A-025  
Scripps Institute of Oceanography  
University of California, San Diego  
La Jolla, CA 92093

Prof. Adam Dziewonski  
Hoffman Laboratory, Harvard University  
Dept. of Earth Atmos. & Planetary Sciences  
20 Oxford Street  
Cambridge, MA 02138

Dr. Jeffrey W. Given  
SAIC  
10260 Campus Point Drive  
San Diego, CA 92121

Prof. John Ebel  
Department of Geology & Geophysics  
Boston College  
Chestnut Hill, MA 02167

Dr. Dale Glover  
Defense Intelligence Agency  
ATTN: ODT-1B  
Washington, DC 20301

Eric Fielding  
SNEE Hall  
INSTOC  
Cornell University  
Ithaca, NY 14853

Dr. Indra Gupta  
Teledyne Geotech  
314 Montgomery Street  
Alexandria, VA 22314

Dr. Mark D. Fisk  
Mission Research Corporation  
735 State Street  
P.O. Drawer 719  
Santa Barbara, CA 93102

Dan N. Hagedorn  
Pacific Northwest Laboratories  
Battelle Boulevard  
Richland, WA 99352

Prof Stanley Flatte  
Applied Sciences Building  
University of California, Santa Cruz  
Santa Cruz, CA 95064

Dr. James Hannon  
Lawrence Livermore National Laboratory  
P.O. Box 808  
L-205  
Livermore, CA 94550

Dr. John Foley  
NER-Geo Sciences  
1100 Crown Colony Drive  
Quincy, MA 02169

Dr. Roger Hansen  
HQ AFTAC/TTR  
Patrick AFB, FL 32925-6001

Prof. Donald Forsyth  
Department of Geological Sciences  
Brown University  
Providence, RI 02912

Prof. David G. Harkrider  
Seismological Laboratory  
Division of Geological & Planetary Sciences  
California Institute of Technology  
Pasadena, CA 91125

Dr. Art Frankel  
U.S. Geological Survey  
922 National Center  
Reston, VA 22092

Prof. Danny Harvey  
CIRES  
University of Colorado  
Boulder, CO 80309

Prof. Donald V. Helmberger  
Seismological Laboratory  
Division of Geological & Planetary Sciences  
California Institute of Technology  
Pasadena, CA 91125

Prof. Eugene Herrin  
Institute for the Study of Earth and Man  
Geophysical Laboratory  
Southern Methodist University  
Dallas, TX 75275

Prof. Robert B. Herrmann  
Department of Earth & Atmospheric Sciences  
St. Louis University  
St. Louis, MO 63156

Prof. Lane R. Johnson  
Seismographic Station  
University of California  
Berkeley, CA 94720

Prof. Thomas H. Jordan  
Department of Earth, Atmospheric &  
Planetary Sciences  
Massachusetts Institute of Technology  
Cambridge, MA 02139

Prof. Alan Kafka  
Department of Geology & Geophysics  
Boston College  
Chestnut Hill, MA 02167

Robert C. Kemerait  
ENSCO, Inc.  
445 Pineda Court  
Melbourne, FL 32940

Dr. Max Koontz  
U.S. Dept. of Energy/DP 5  
Forrestal Building  
1000 Independence Avenue  
Washington, DC 20585

Dr. Richard LaCoss  
MIT Lincoln Laboratory, M-200B  
P.O. Box 73  
Lexington, MA 02173-0073

Dr. Fred K. Lamb  
University of Illinois at Urbana-Champaign  
Department of Physics  
1110 West Green Street  
Urbana, IL 61801

Prof. Charles A. Langston  
Geosciences Department  
403 Deike Building  
The Pennsylvania State University  
University Park, PA 16802

Jim Lawson, Chief Geophysicist  
Oklahoma Geological Survey  
Oklahoma Geophysical Observatory  
P.O. Box 8  
Leonard, OK 74043-0008

Prof. Thorne Lay  
Institute of Tectonics  
Earth Science Board  
University of California, Santa Cruz  
Santa Cruz, CA 95064

Dr. William Leith  
U.S. Geological Survey  
Mail Stop 928  
Reston, VA 22092

Mr. James F. Lewkowicz  
Phillips Laboratory/GPEH  
Hanscom AFB, MA 01731-5000( 2 copies)

Mr. Alfred Lieberman  
ACDA/VI-OA State Department Building  
Room 5726  
320-21st Street, NW  
Washington, DC 20451

Prof. L. Timothy Long  
School of Geophysical Sciences  
Georgia Institute of Technology  
Atlanta, GA 30332

Dr. Randolph Martin, III  
New England Research, Inc.  
76 Olcott Drive  
White River Junction, VT 05001

Dr. Robert Masse  
Denver Federal Building  
Box 25046, Mail Stop 967  
Denver, CO 80225

Dr. Gary McCartor  
Department of Physics  
Southern Methodist University  
Dallas, TX 75275

Prof. Thomas V. McEvilly  
Seismographic Station  
University of California  
Berkeley, CA 94720

Dr. Art McGarr  
U.S. Geological Survey  
Mail Stop 977  
U.S. Geological Survey  
Menlo Park, CA 94025

Dr. Keith L. McLaughlin  
S-CUBED  
A Division of Maxwell Laboratory  
P.O. Box 1620  
La Jolla, CA 92038-1620

Stephen Miller & Dr. Alexander Florence  
SRI International  
333 Ravenswood Avenue  
Box AF 116  
Menlo Park, CA 94025-3493

Prof. Bernard Minster  
IGPP, A-025  
Scripps Institute of Oceanography  
University of California, San Diego  
La Jolla, CA 92093

Prof. Brian J. Mitchell  
Department of Earth & Atmospheric Sciences  
St. Louis University  
St. Louis, MO 63156

Mr. Jack Murphy  
S-CUBED  
A Division of Maxwell Laboratory  
11800 Sunrise Valley Drive, Suite 1212  
Reston, VA 22091 (2 Copies)

Dr. Keith K. Nakanishi  
Lawrence Livermore National Laboratory  
L-025  
P.O. Box 808  
Livermore, CA 94550

Dr. Carl Newton  
Los Alamos National Laboratory  
P.O. Box 1663  
Mail Stop C335, Group ESS-3  
Los Alamos, NM 87545

Dr. Bao Nguyen  
HQ AFTAC/TTR  
Patrick AFB, FL 32925-6001

Prof. John A. Orcutt  
IGPP, A-025  
Scripps Institute of Oceanography  
University of California, San Diego  
La Jolla, CA 92093

Prof. Jeffrey Park  
Kline Geology Laboratory  
P.O. Box 6666  
New Haven, CT 06511-8130

Dr. Howard Patton  
Lawrence Livermore National Laboratory  
L-025  
P.O. Box 808  
Livermore, CA 94550

Dr. Frank Pilotte  
HQ AFTAC/TT  
Patrick AFB, FL 32925-6001

Dr. Jay J. Pulli  
Radix Systems, Inc.  
2 Taft Court, Suite 203  
Rockville, MD 20850

Dr. Robert Reinke  
ATTN: FCTVTD  
Field Command  
Defense Nuclear Agency  
Kirtland AFB, NM 87115

Prof. Paul G. Richards  
Lamont-Doherty Geological Observatory  
of Columbia University  
Palisades, NY 10964

Mr. Wilmer Rivers  
Teledyne Geotech  
314 Montgomery Street  
Alexandria, VA 22314

Dr. George Rothe  
HQ AFTAC/TTR  
Patrick AFB, FL 32925-6001

Dr. Alan S. Ryall, Jr.  
DARPA/NMRO  
3701 North Fairfax Drive  
Arlington, VA 22209-1714



Dr. Richard Sailor  
TASC, Inc.  
55 Walkers Brook Drive  
Reading, MA 01867

Prof. Charles G. Sammis  
Center for Earth Sciences  
University of Southern California  
University Park  
Los Angeles, CA 90089-0741

Prof. Christopher H. Scholz  
Lamont-Doherty Geological Observatory  
of Columbia University  
Palisades, CA 10964

Dr. Susan Schwartz  
Institute of Tectonics  
1156 High Street  
Santa Cruz, CA 95064

Secretary of the Air Force  
(SAFRD)  
Washington, DC 20330

Office of the Secretary of Defense  
DDR&E  
Washington, DC 20330

Thomas J. Sereno, Jr.  
Science Application Int'l Corp.  
10260 Campus Point Drive  
San Diego, CA 92121

Dr. Michael Shore  
Defense Nuclear Agency/SPSS  
6801 Telegraph Road  
Alexandria, VA 22310

Dr. Matthew Sibol  
Virginia Tech  
Seismological Observatory  
4044 Derring Hall  
Blacksburg, VA 24061-0420

Prof. David G. Simpson  
IRIS, Inc.  
1616 North Fort Myer Drive  
Suite 1440  
Arlington, VA 22209

Donald L. Springer  
Lawrence Livermore National Laboratory  
L-025  
P.O. Box 808  
Livermore, CA 94550

Dr. Jeffrey Stevens  
S-CUBED  
A Division of Maxwell Laboratory  
P.O. Box 1620  
La Jolla, CA 92038-1620

Lt. Col. Jim Stobie  
ATTN: AFOSR/NL  
Bolling AFB  
Washington, DC 20332-6448

Prof. Brian Stump  
Institute for the Study of Earth & Man  
Geophysical Laboratory  
Southern Methodist University  
Dallas, TX 75275

Prof. Jeremiah Sullivan  
University of Illinois at Urbana-Champaign  
Department of Physics  
1110 West Green Street  
Urbana, IL 61801

Prof. L. Sykes  
Lamont-Doherty Geological Observatory  
of Columbia University  
Palisades, NY 10964

Dr. David Taylor  
ENSCO, Inc.  
445 Pineda Court  
Melbourne, FL 32940

Dr. Steven R. Taylor  
Los Alamos National Laboratory  
P.O. Box 1663  
Mail Stop C335  
Los Alamos, NM 87545

Prof. Clifford Thurber  
University of Wisconsin-Madison  
Department of Geology & Geophysics  
1215 West Dayton Street  
Madison, WS 53706

Prof. M. Nafi Toksoz  
Earth Resources Lab  
Massachusetts Institute of Technology  
42 Carleton Street  
Cambridge, MA 02142

Dr. Larry Turnbull  
CIA-OSWR/NED  
Washington, DC 20505

DARPA/RMO/SECURITY OFFICE  
3701 North Fairfax Drive  
Arlington, VA 22203-1714

Dr. Gregory van der Vink  
IRIS, Inc.  
1616 North Fort Myer Drive  
Suite 1440  
Arlington, VA 22209

HQ DNA  
ATTN: Technical Library  
Washington, DC 20305

Dr. Karl Veith  
EG&G  
5211 Auth Road  
Suite 240  
Suitland, MD 20746

Defense Intelligence Agency  
Directorate for Scientific & Technical Intelligence  
ATTN: DTIB  
Washington, DC 20340-6158

Prof. Terry C. Wallace  
Department of Geosciences  
Building #77  
University of Arizona  
Tuscon, AZ 85721

Defense Technical Information Center  
Cameron Station  
Alexandria, VA 22314 (2 Copies)

Dr. Thomas Weaver  
Los Alamos National Laboratory  
P.O. Box 1663  
Mail Stop C335  
Los Alamos, NM 87545

TACTEC  
Battelle Memorial Institute  
505 King Avenue  
Columbus, OH 43201 (Final Report)

Dr. William Wortman  
Mission Research Corporation  
8560 Cinderbed Road  
Suite 700  
Newington, VA 22122

Phillips Laboratory  
ATTN: XPG  
Hanscom AFB, MA 01731-5000

Prof. Francis T. Wu  
Department of Geological Sciences  
State University of New York  
at Binghamton  
Vestal, NY 13901

Phillips Laboratory  
ATTN: GPE  
Hanscom AFB, MA 01731-5000

AFTAC/CA  
(STINFO)  
Patrick AFB, FL 32925-6001

Phillips Laboratory  
ATTN: TSML  
Hanscom AFB, MA 01731-5000

DARPA/PM  
3701 North Fairfax Drive  
Arlington, VA 22203-1714

Phillips Laboratory  
ATTN: SUL  
Kirtland, NM 87117 (2 copies)

DARPA/RMO/RETRIEVAL  
3701 North Fairfax Drive  
Arlington, VA 22203-1714

Dr. Michel Bouchon  
I.R.I.G.M.-B.P. 68  
38402 St. Martin D'Heres  
Cedex, FRANCE

Dr. Michel Campillo  
Observatoire de Grenoble  
I.R.I.G.M.-B.P. 53  
38041 Grenoble, FRANCE

Dr. Jorg Schlittenhardt  
Federal Institute for Geosciences & Nat'l Res.  
Postfach 510153  
D-3000 Hannover 51, GERMANY

Dr. Kin Yip Chun  
Geophysics Division  
Physics Department  
University of Toronto  
Ontario, CANADA

Dr. Johannes Schweitzer  
Institute of Geophysics  
Ruhr University/Bochum  
P.O. Box 1102148  
4360 Bochum 1, GERMANY

Prof. Hans-Peter Harjes  
Institute for Geophysics  
Ruhr University/Bochum  
P.O. Box 102148  
4630 Bochum 1, GERMANY

Prof. Eystein Husebye  
NTNF/NORSAR  
P.O. Box 51  
N-2007 Kjeller, NORWAY

David Jepsen  
Acting Head, Nuclear Monitoring Section  
Bureau of Mineral Resources  
Geology and Geophysics  
G.P.O. Box 378, Canberra, AUSTRALIA

Ms. Eva Johannisson  
Senior Research Officer  
National Defense Research Inst.  
P.O. Box 27322  
S-102 54 Stockholm, SWEDEN

Dr. Peter Marshall  
Procurement Executive  
Ministry of Defense  
Blacknest, Brimpton  
Reading FG7-FRS, UNITED KINGDOM

Dr. Bernard Massinon, Dr. Pierre Mechler  
Societe Radiomana  
27 rue Claude Bernard  
75005 Paris, FRANCE (2 Copies)

Dr. Svein Mykkeltveit  
NTNF/NORSAR  
P.O. Box 51  
N-2007 Kjeller, NORWAY (3 Copies)

Prof. Keith Priestley  
University of Cambridge  
Bullard Labs, Dept. of Earth Sciences  
Madingley Rise, Madingley Road  
Cambridge CB3 0EZ, ENGLAND